STUDY OF ACOUSTIC-GRAVITY WAVE GENERATION BY NUCLEAR DETONATIONS

By

S. L. Kahalas
T. I. McLaren
B. L. Murphy

MT. AUBURN RESEARCH ASSOCIATES, INC.
385 Elliot Street
Newton Upper Falls, Massachusetts 02164

Sponsored by

Advanced Research Projects Agency
ARPA Order No. 1502, Amendment No. 2

Monitored by

Air Force Office of Scientific Research

Program Code:	1F10
Effective Date of Contract:	16 February 1971
Contract Expiration Date:	15 April 1972
Amount of Contract Dollars:	$78,441.00
Contract No:	F44620-71-C-0086
Principal Investigator:	Dr. Brian L. Murphy
Telephone Number:	(617) 969-7150
Type of Report:	Final
Period Covered:	16 February 1971 through 15 February 1972

15 April 1972

STUDY OF ACOUSTIC-GRAVITY WAVE GENERATION BY NUCLEAR DETONATIONS

By

S. L. Kahalas
T. I. McLaren
B. L. Murphy

MT. AUBURN RESEARCH ASSOCIATES, INC.
385 Elliot Street
Newton Upper Falls, Massachusetts 02164

Sponsored by

Advanced Research Projects Agency
ARPA Order No. 1502, Amendment No. 2

Monitored by

Air Force Office of Scientific Research

Program Code:	1F10
Effective Date of Contract:	16 February 1971
Contract Expiration Date:	15 April 1972
Amount of Contract Dollars:	$78,441.00
Contract No:	F44620-71-C-0086
Principal Investigator:	Dr. Brian L. Murphy
Telephone Number:	(617) 969-7150
Type of Report:	Final
Period Covered:	16 February 1971 through 15 February 1972

15 April 1972

Unclassified

Security Classification

DOCUMENT CONTROL DATA - R & D

(Security classification of title, body of abstract and indexing annotation must be entered when the overall report is classified)

1. ORIGINATING ACTIVITY *(Corporate author)*
MT. AUBURN RESEARCH ASSOCIATES, INC.
385 Elliot Street
Newton, Massachusetts 02164

2a. REPORT SECURITY CLASSIFICATION
Unclassified

2b. GROUP

3. REPORT TITLE
A STUDY OF ACOUSTIC-GRAVITY WAVE GENERATION BY NUCLEAR DETONATIONS

4. DESCRIPTIVE NOTES *(Type of report and inclusive dates)*
Final Report (16 Feb 71 - 15 Feb 72)

5. AUTHOR(S) *(First name, middle initial, last name)*
S. L. Kahalas, T. I. McLaren, B. L. Murphy

6. REPORT DATE	7a. TOTAL NO. OF PAGES	7b. NO. OF REFS
15 April 1972	84	29

8a. CONTRACT OR GRANT NO.	9a. ORIGINATOR'S REPORT NUMBER(S)
F44620-71-C-0086	
b. PROJECT NO. AO 1502	
c. 62701D	9b. OTHER REPORT NO(S) *(Any other numbers that may be assigned this report)* AFOSR - TR - 72 - 1331
d.	

10. DISTRIBUTION STATEMENT
Approved for public release; distribution unlimited.

11. SUPPLEMENTARY NOTES	12. SPONSORING MILITARY ACTIVITY
Tech, Other	Air Force Office of Scientific Research 1400 Wilson Boulevard (NPG) Arlington, Virginia 22209

13. ABSTRACT

Conclusions based on previous work done on the contract and published in detail elsewhere are first reviewed. This earlier work treated the generation and propagation of both long period (3-10 minutes) and short period (1-60 seconds) acoustic signals from nuclear detonations. Also included in the review are conclusions reached concerning Rayleigh wave generation by atmospheric explosions.

Recent work, reported for the first time, is then described. This consists of: (a) An analysis of the relationship of different kinds of disturbance seen in the ionosphere to the hydrodynamic motions accompanying a low altitude nuclear explosion. Both the detonation blast wave and the buoyant rising fireball are considered as sources of ionospheric disturbance. (b) A laboratory investigation of the internal gravity waves generated by buoyant rise in a density stratified medium.

DD FORM 1 NOV 68 1473 REPLACES DD FORM 1473, 1 JAN 64, WHICH IS OBSOLETE FOR ARMY USE.

Unclassified

Security Classification

14. KEY WORDS	LINK A		LINK B		LINK C	
	ROLE	WT	ROLE	WT	ROLE	WT
Acoustic-gravity waves						
Buoyant release experiments						
Ionospheric effects						
Nuclear explosions						

ACKNOWLEDGEMENTS

Major contributions to the theoretical analysis in Section 4 were made by Professor A. D. Pierce and the original conception for the laboratory experiment described in that section was in large part due to Dr. T. Fohl.

TABLE OF CONTENTS

LIST OF FIGURES - Section 3

LIST OF FIGURES - Section 4

1. INTRODUCTION

Work performed on this contract has been concerned with acoustic disturbances which are relevant to the problem of long-range detection and diagnosis of atmospheric nuclear explosions. Our earlier work concentrated on acoustic signals which originate in the detonation blast wave and which can be detected on the ground by microbarographs or seismometers. More recently we have investigated the rising fireball as a source of acoustic signals and have turned our attention to acoustic signals in the ionosphere which can be detected by electromagnetic methods.

In Section 2, conclusions reached during our earlier work on the contract are reviewed. This work is described in detail in our Semi-Annual Report.* Three different acoustic phenomena relevant to nuclear test detection and diagnostics were discussed in this report: (1) The generation of long period (3-10 minute) acoustic-gravity waves was analyzed in terms of a Lamb mode propagation theory. One result of the analysis was that yield-amplitude proportionality was predicted to break down for very large yield detonations. (2) The generation and propagation of short period (1-60 seconds) acoustic pulses was treated by means of weak shock theory. Yield and height of burst scaling laws were derived for the far-field period. The dependence of period on atmospheric conditions and propagation path was also discussed. (3) The variation of long range Rayleigh wave amplitude with yield and height of burst was discussed for atmospheric explosions.

In Section 3, the relationship between hydrodynamic motions caused by a low altitude nuclear explosion and subsequent ionospheric disturbances is reviewed. Both the upward going shock and the rising fireball are considered as hydrodynamic sources. It is shown that different portions of the shock front may be classified in terms of

---

* B. L. Murphy and A. D. Zalay, "Study of Acoustic-Gravity Wave Generation by Nuclear Detonations," Mt. Auburn Research Associates, Inc. Report under AFOSR Contract No. F44620-71-C-0086, 30 September 1971.

the ionospheric disturbance they create. The portion of the shock front reflected from the 100-120 km altitude level produces disturbance periods the order of a minute for a megaton detonation. The portion of the shock front which propagates above the 100-120 km level is responsible, through a complex nonlinear process, for disturbance periods in excess of 10 minutes. It is shown that the fireball is most efficient in generating acoustic-gravity waves when it reaches its stabilization altitude and approaches hydrodynamic equilibrium with the atmosphere. Theory and laboratory experiment indicate that the fireball then produces a wave spectrum peaked at periods slightly longer than the ambient Brunt-Väisälä period (≈ 5 minutes).

In Section 4, laboratory experiments are described which are intended to simulate gravity waves generated by the rise and stabilization of a fireball. Observations were made of the internal waves generated in a density stratified fluid by the motion of a buoyantly rising miscible fluid. The gravity wave motions were analyzed by observing the trajectories followed by small neutrally buoyant beads dispersed throughout the stratified medium and good agreement was found with theoretical predictions. It was confirmed that a source of frequency ω oscillating in a medium whose Brunt-Väisälä frequency is ω_o tends to radiate mainly at an inclination θ to the vertical given by $\theta \approx \cos^{-1}\left(\frac{\omega}{\omega_o}\right)$. It was observed that the rise time of a buoyant fluid to its stabilization height was about 0.85 times the Brunt period, and that the fluid typically undergoes about two oscillations before coming to rest vertically. The gravity wave field for a buoyant release experiment was observed to be inhomogeneous, covering a range of frequencies, but in general $\omega_o \geq \omega \geq \omega_o/2$. It was clear that gravity waves were generated mainly by the oscillatory motion of the fluid around its stabilization height, rather than during its rise. Finally, it was shown that if measurements are made of only two characteristics of fluid particle trajectories, viz.: the inclination

of the major axis of particle motion, and the ratio of major to minor axis for its (in general) elliptical orbit, then it is possible to identify the location of an unseen source of internal gravity waves.

Overall conclusions reached are presented in Section 5.

2. REVIEW OF PREVIOUS WORK ON THE CONTRACT

Three different kinds of acoustic phenomena related to nuclear test detection and diagnostics were discussed in the Semi-Annual Report.* They are: (1) Long period (3-10 minutes) acoustic-gravity waves which propagate in the real atmosphere's counterpart to Lamb's edge mode. (2) High frequency (1-60 second period) acoustic pulses which result from the degeneration of the detonation blast wave into a weak shock. (3) Rayleigh or surface seismic waves which result when the detonation shock wave strikes the earth. Conclusions reached for each of these phenomena are given below.

2.1 LAMB MODE ANALYSIS

(a) The shock front extending from the ground to many scale heights above the ground was found to be of almost equal importance in determining the far-field Lamb mode amplitude. Because of this, the far-field amplitude should be relatively independent of phenomena peculiar to any small portion of the shock front. In particular, ground effects such as the presence of a precursor should not play a very important role.

(b) For large yield, low altitude detonations we found a far-field amplitude dependence which varies as $Y\left[1 + \frac{\sqrt{2}}{3}\sqrt{\ell n \frac{Y}{Y^*}}\right]$, where typically Y* is the order of 10 MT for a sea level detonation. This dependence arises from a detailed consideration of the mechanism by which the low frequency components of the near-field (shock) disturbance become spatially separated from the high frequency components. The precise value of the critical yield Y* where yield-amplitude proportionality breaks down is determined by atmospheric conditions near the burst as well as the direction of propagation and must be determined by detailed numerical calculations.

---

* B. L. Murphy and A. D. Zalay, "Study of Acoustic-Gravity Wave Generation by Nuclear Detonations," Mt. Auburn Research Associates, Inc. Report under AFOSR Contract No. F44620-71-C-0086, 30 September 1971.

2.2 HIGH FREQUENCY ACOUSTIC PERIODS

(a) At large distances the dominant acoustic pulse period for a 1 KT detonation was found to be the order of 10 seconds.

(b) For small yields the period was found to scale as $(\text{yield})^{1/3}$. For large yields the scaling is uncertain. The interaction of the rising fireball from high-yield detonations with the upward going shock needs to be investigated before the large yield scaling can be determined.

(c) The range dependence of far-field periods was found to be extremely weak, as an absolute maximum about a 17% increase in going from 2,000 to 10,000 km. Pulse splitting by wind ducts and the effects of other small scale meteorological phenomena are expected to make the actual dependence even weaker than the above value.

(d) The period dependence on height of burst was also found to be extremely weak. The dependence is given approximately as: $T\alpha\left(1 + \frac{\bar{z}}{45.7}\right)$, where T is the period and $\bar{z}$ is the burst height in km.

(e) Probably the most significant variation in far-field period, other than that caused by variations in yield, was found to be caused by the direction of signal propagation relative to the winds at about 50 km altitude. For downwind propagation the signal reflection occurs at a lower altitude than for crosswind or upwind propagation. The dependence of period on reflection altitude was approximately given by: $T \alpha e^{z_o/28}$, where z_o is the reflection altitude in kilometers. A 10 km variation in z_o produces about a 40% variation in T. The altitude z_o can be determined by ray tracing for the appropriate atmospheric conditions and direction of propagation.

2.3 RAYLEIGH WAVE AMPLITUDES

Our detailed conclusions are contained in the Semi-Annual Report in the form of plots of source strength for Rayleigh wave excitation vs yield and height of burst. Some general conclusions were as follows:

(a) The source strength, which contains all the yield and height of burst dependence for the far-field amplitudes, was found to increase less rapidly with yield Y the higher the burst altitude. For example, for a Rayleigh wave period of 20 sec and for yields between 100 and 500 KT we found $S \alpha Y^{.93}$ for detonations at 2km altitude, $S \alpha Y^{.89}$ at 5 km, $S \alpha Y^{.68}$ at 10 km, and $S \alpha Y^{.61}$ at 40 km.

(b) For large yields and short Rayleigh wave periods τ (for example, Y > 500 KT for τ = 10 sec) the source strength was found to be a monotonic decreasing function of height of burst. For larger yields or longer Rayleigh wave periods S was maximized for a particular height of burst. The altitude at which the maximum occurred increased with increasing τ and decreasing Y. For Y = 1 MT and τ = 20 sec the maximum occurred at about 45 km altitude.

(c) The variation of S with height of burst was appreciable. For example, for τ = 20 sec and Y = 100 KT, S increased by a factor of 2.3 as the height of burst was raised from 4 km to 20 km.

3. MODELING OF NUCLEAR SOURCES OF ACOUSTIC-GRAVITY WAVES*

3.1 INTRODUCTION

It is known that large yield nuclear explosions result in ionospheric disturbances which can be observed by electromagnetic means at great distances from the explosion site. It is also widely recognized that these disturbances are a result of acoustic-gravity waves whose propagation is supported by the neutral fluid component of the ionosphere. A recent bibliography contains many references to observations and theory relating to detonation produced disturbances (THOMAS, J. E., et al., 1972).

Much of the previous theoretical development deals with wave propagation rather than source modeling. It is to the latter topic that this paper is devoted. In the subsequent discussion we outline how the hydrodynamic motions near a nuclear detonation result in the generation of acoustic-gravity waves and how the properties of these waves are determined by the explosion parameters. That is, how onset time, amplitude, and period of the ionospheric disturbance are related to explosion yield and height of burst.

Because we concentrate on source modeling, we will not discuss wave propagation except insofar as it is necessary to do so to relate theoretical predictions to observations. Similarly, we do not consider how the neutral fluid motions determine ionospheric electron densities and hence the ultimate electromagnetic effect. This difficult problem has been treated by a number of authors (for example, HOOKE, W. H., 1968).

Our treatment is limited to low altitude detonations where the initial energy deposition may be assumed to be local and spherically symmetric. For this type of detonation both the shock and the fireball can generate acoustic-gravity waves. The mechanisms which will be discussed are as follows:

a. The direct effects of the shock are manifest as ionospheric signals with periods the order of a minute for a megaton detonation, the period being determined by the positive phase duration of the shock when it reaches the ionospheric

* Paper to be presented at the EPP-AGARD Specialist Meeting on "Effects of Atmospheric Gravity Waves on Electromagnetic Wave Propagation," at Wiesbaden, Germany 17-21 April 1972.

level. The acoustic signal in this case undergoes multiple reflections between the ground and the base of the ionosphere. The ducting is imperfect at the upper level and energy continuously leaks into the ionosphere.

b. In addition, the short period (order of a minute) hydrodynamic motions that characterize the shock as it enters the ionosphere above the burst evolve into long period (10 minutes and more) disturbances through a highly nonlinear process occurring at the 100-120 km altitude level. This phenomenon, which has been demonstrated by numerical calculations (GREENE, J. S., Jr. and W. A. WHITAKER, 1968), involves a refraction and folding over of the shock due to the rapid change in ambient temperature at this level. Long period wave propagation due to this mechanism commences at 10 minutes or more after the detonation. This time, which is when the effective excitation appears to have begun according to a distant observer, is the time required for the shock to reach the ionospheric level and for the long period fluid motions to become established.

c. The fireball is most efficient in generating acoustic-gravity waves when it has reached its terminal or stabilization altitude. It then approaches hydrodynamic equilibrium with the atmosphere on a time scale comparable with the Brunt-Väisälä period, the natural oscillation period of the atmosphere. This is also approximately the time required for the fireball to reach its terminal altitude and wave generation to begin. For, as will be shown, the fireball is not an efficient emitter of waves during the early portions of its rise.

Acoustic-gravity wave generation during fireball terminal phase has been modeled in the laboratory and these experimental studies will be described.

As shown below, for megaton range detonations the energy available for wave generation by the fireball is comparable to the energy available for long period wave generation by the shock. However, the dominant frequency of the waves generated by fireball stabilization is only slightly less than the Brunt-Väisälä frequency and waves of this frequency propagate at relatively steep angles to the horizontal. For this reason the fireball mechanism may only be capable of producing ionospheric disturbances in the immediate vicinity of the burst location.

These general remarks are discussed in more detail in the succeeding sections. We first discuss the shock and then the fireball mechanism. We then assess the importance of these mechanisms in terms of the resulting ionospheric effects.

3.2 SHOCK WAVE GENERATION OF ACOUSTIC-GRAVITY WAVES

It is useful to first consider the propagation of the shock front as it is refracted by the atmosphere. Different portions of the shock are refracted differently. This leads to a classification of different portions of the shock front in terms of the types of ionospheric disturbance that they create.

At some distance from the burst point the shock becomes weak, that is, the relative overpressure $\Delta P/P$ becomes much less than unity. ΔP is the overpressure and P is the ambient pressure. For example, for a megaton detonation $\Delta P/P = .1$ at about 9 km (LEHTO, D. L. and R. A. LARSON, 1969). When the shock becomes weak the effects of atmospheric stratification and winds become important.

An example of ray tracing calculations for a realistic (but windless) atmosphere is shown in Figure 1 (BARRY, G., 1963) for a source located at the ground. The figure does not include any nonacoustic propagation effects such as those arising near the source where the shock is strong. The initial ray angles in Figure 1 start at zero degrees to the horizontal and increase in 5° increments. The ultimate behavior of different portions of the shock front is determined by the initial angle of propagation relative to the horizontal as indicated in Figure 1. As

FIGURE 1. Acoustic Ray Tracing for a Sea-level Source. Initial Ray Angle Begin with 0^{o} from the Horizontal and Increase by 5^{o} Increments.

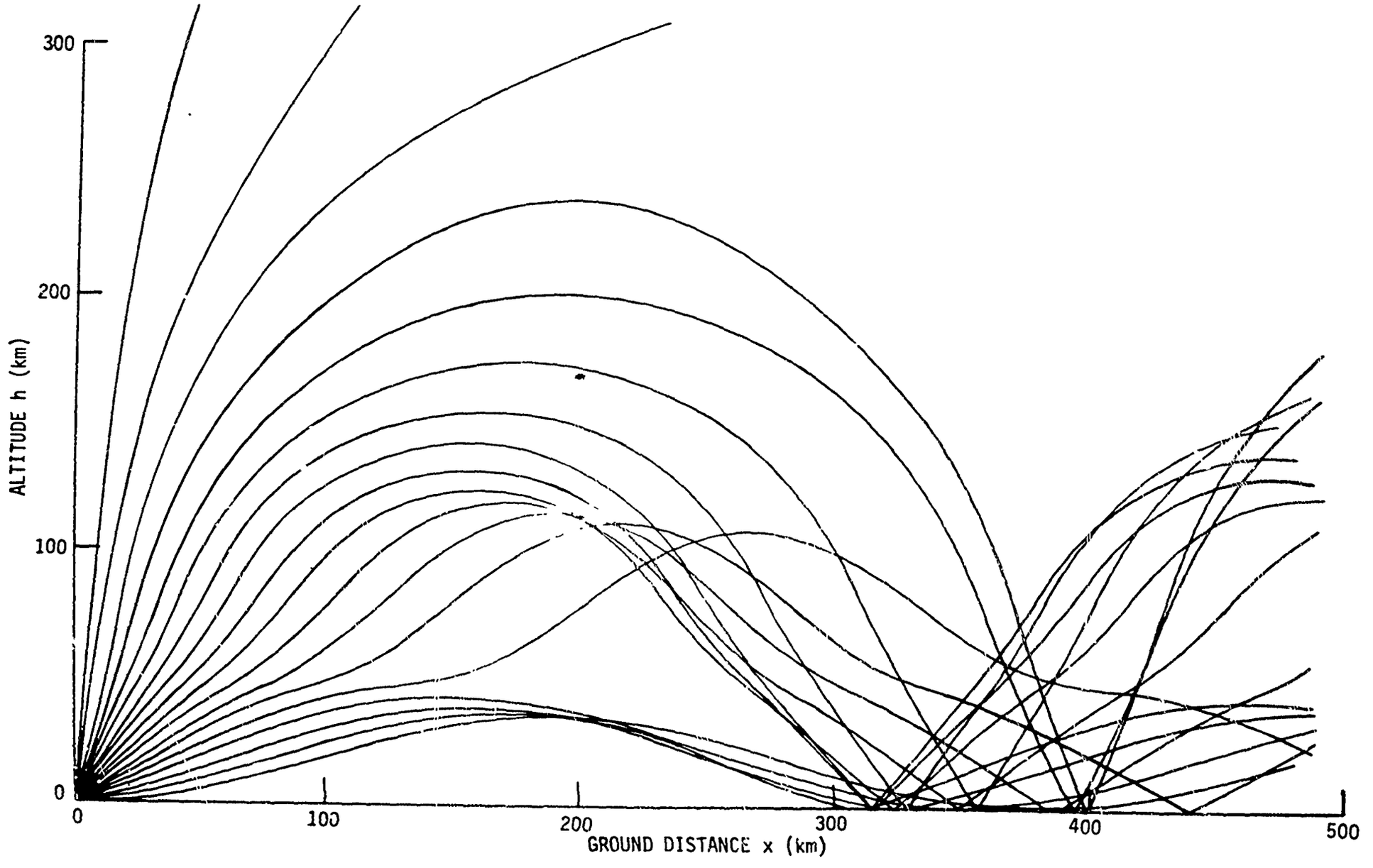

this angle is increased the different types of disturbance are:

a. Acoustic disturbances reflected back toward the earth before reaching the ionosphere. In Figure 1 this corresponds to initial angles of less than 20°. This type of signal may undergo repeated reflections between the ground and some higher level, in Figure 1 the 40 km region of the stratosphere, where suitable temperature and wind conditions exist. When this portion of the shock front becomes weak it may be repeatedly split by winds resulting in a mutipulse type of infrasonic signal (MEECHAM, W. C., 1968).

b. The direct shock which reaches the 100-120 km level of the ionosphere before being reflected at the region of very sharp temperature increase. This signal, which corresponds to the interval from 20° to perhaps 35° in Figure 1, can be ducted between the base of the ionosphere and the ground as shown. As discussed below, leakage from the upper portion of the duct to the ionosphere is probably responsible for acoustic-wave disturbances observed in the ionosphere (BAKER, D. M. and K. Davies, 1968).

c. A portion of the shock front which propagates into the thermosphere beyond the 100-120 km level. This corresponds to angles of more than about 35° in Figure 1. Numerical calculations of the nonlinear hydrodynamics done by Greene and Whitaker (1968), which are discussed below, show that this portion of the shock loses much of its energy in the creation of a horizontally propagating disturbance behind the front.

   This disturbance is believed to be responsible for the very long period ionospheric perturbations observed at great distances following large yield explosions.

Our concern in the following is with the portion of the shock front which reaches the 100-120 km altitude level. Throughout, only

the primary shock wave is considered and secondary shocks due to reflection from the fireball or the ground are neglected.

We first determine the properties of the upward going shock at the 100-120 km altitude level. We then discuss the relationship of these shock properties to the properties of short period ionospheric disturbances. Finally we discuss the nonlinear process at the 100-120 km level which results in the generation of long period ionospheric disturbances.

3.2.1 The Upward Going Shock

In this section we will calculate the relative overpressure and the positive phase duration of the shock at the base of the ionosphere as functions of yield and height of burst. These results are subsequently used to relate ionospheric disturbance properties to explosion parameters. To determine the properties of the upward going shock a simplified scaling law known as modified Sachs scaling is used (LUTZKY, M. and D. L. Lehto, 1968) together with weak shock theory (REED, S. G., Jr., 1959).

According to modified Sachs scaling the relative overpressure, in an inhomogeneous atmosphere, at a distance r from an explosion where the ambient pressure is P(r), is just the same as if the explosion had occurred in a homogeneous atmosphere with ambient pressure P(r). That is:

$$\frac{\Delta P}{P(r)} = f\left\{r\left[\frac{P(r)}{Y}\right]^{1/3}\right\} \qquad (1)$$

where Y is the explosion yield and f is the function which gives the relative overpressure in a homogeneous atmosphere. An example of the application of modified Sachs scaling is shown in Figure 2 where we compare the predictions of this scaling with the results of SAP and SHELL calculations for relative overpressure versus distance. SAP is a one dimensional Lagrangian hydrodynamic code and SHELL is a two dimensional Eulerian hydrodynamic code. These calculations are for shock propagation at 45^{o} from the horizontal due to a 4 MT isothermal sphere at 5 km altitude (GREENE, J. S., Jr., personal communication, 1971). The modified Sachs scaling curve has been constructed using

FIGURE 2. Comparison of SHELL and SAP Codes at 45° with Modified Sachs Scaling for 4 MT at 5 km. After GREENE and WHITAKER (1968).

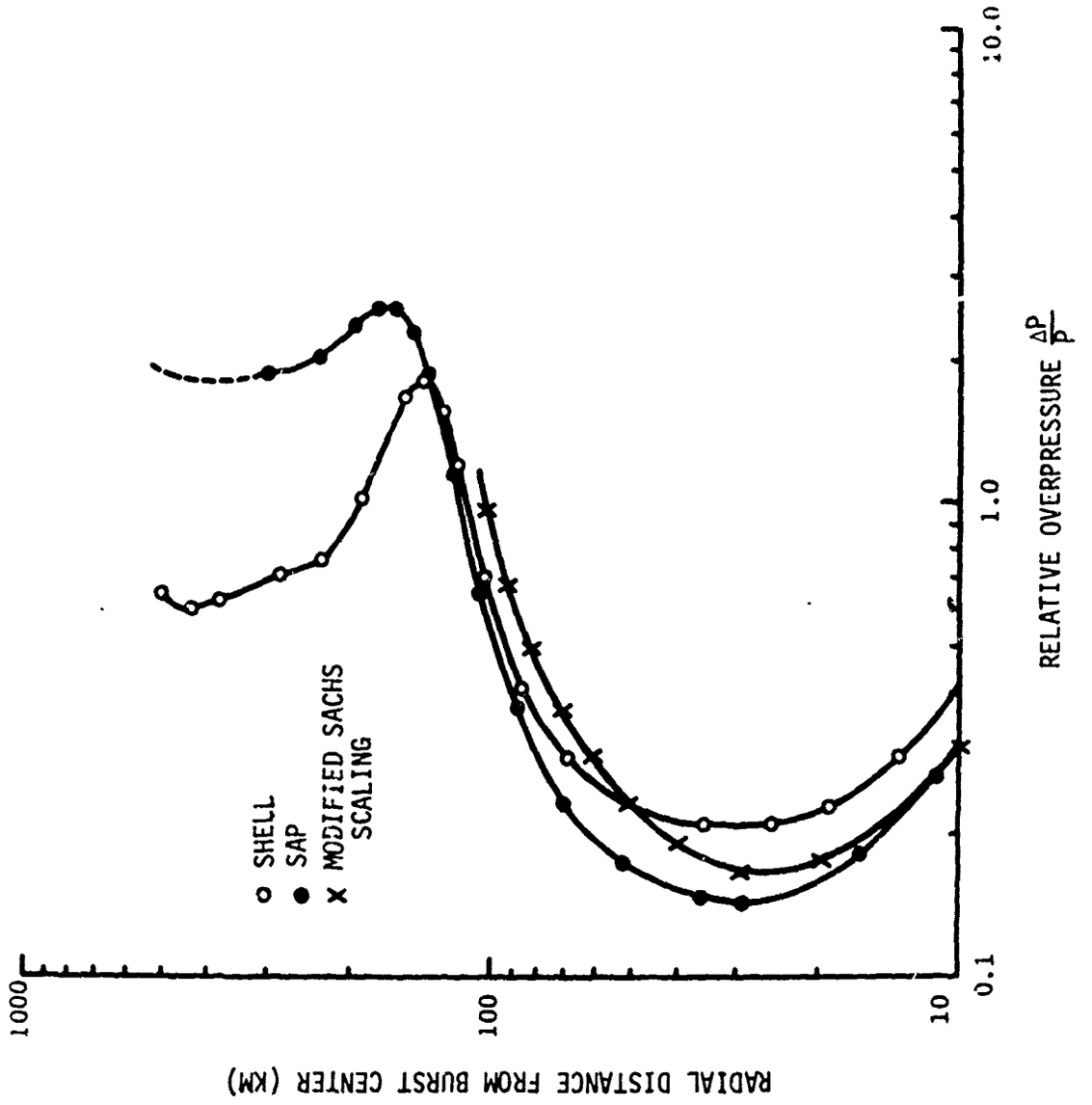

the 1962 Standard atmosphere for the ambient pressure P(r) and the homogeneous atmosphere, real air, calculations of Lehto and Larson (1969) for the function f accurring in Eq. (1).

Notice that the SHELL calculation consistently gives somewhat higher relative overpressures below 100 km altitude than does SAP. This is because it includes the effects of fireball rise which SAP does not. The rising fireball, particularly for large yields, prevents the shock from relieving backwards. At very small angles from the horizontal the differences between SHELL and SAP are negligible. Both SHELL and SAP show a drop in relative overpressure commencing at about 100 km altitude. The reason for this and its relation to acoustic-gravity wave generation at the ionospheric level will be discussed shortly. First we continue the discussion of modified Sachs scaling and the upward shock propagation.

It is not entirely clear why modified Sachs scaling works as well as it does. However, in this example, as well as in others not shown here, modified Sachs scaling is definitely more accurate than scaling of distance with respect to ambient pressure at the detonation altitude. Because modified Sachs scaling is expected to become more inaccurate with increasing distance, we use it only to obtain starting values near the burst point for the application of weak shock theory. In using weak shock theory to obtain scaling laws for the shock properties on entering the ionospheric level we make two simplifying assumptions: First, that the atmosphere can be approximated as exponential. Second, that in spite of refractive effects, each portion of the shock front propagates independently with its own effective radius of curvature. These assumptions are justified by the fact that we treat shock propagation in the atmosphere below 120 km altitude where the scale height is approximately constant and by the fact that we only consider the portion of the shock front which is not seriously refracted (i.e. reflected) before reaching the altitude in question.

For reasons which appear below we begin using weak shock theory at a distance r_o where $\Delta P/P = \Delta P_o/P_o$ first equals 0.2. Assuming that the atmosphere near the burst may be approximated as exponential this value of the function f occurring in Eq. (1) corresponds to (LEHTO, D. L. and

R. A. LARSON, 1969):

$$r_o e^{-r_o/3H} = .53 \left(\frac{Y}{P_b}\right)^{1/3} \text{km}, \tag{2}$$

where Y is the yield in kilotons, and P_b is the ambient pressure at the burst point in atmospheres. H is the effective scale height in kilmeters for the (upward) direction being considered.

At distances $r > r_o$ we use the weak shock equations derived by Reed (1959). These are:

$$\frac{\Delta P}{P} = \frac{\Delta P_o}{P_o} \frac{r_o}{r} \frac{t_+^o}{t_+} \sqrt{\frac{P(r_o)}{P(r)}} \tag{3}$$

$$\frac{t_+}{t_+^o} = \left[1 + \frac{\gamma + 1}{2\gamma} \frac{\Delta P_o}{P_o} \frac{r_o}{c\, t_+^o} \int_{r_o}^{r} \sqrt{\frac{P(r_o)}{P(r)}} \frac{dr}{r}\right]^{\frac{1}{2}} \tag{4}$$

where t_+ is the positive phase duration of the shock, γ is the ratio of specific heats, and c is the speed of sound. Nonlinear (weak shock) effects are contained in Eq. (3) within the factor t_+^o/t_+. This factor as given by Eq. (4) includes both the effects of dissipation at the shock front and positive phase lengthening due to the supersonic front velocity.

The dependence of t_+ on values at r_o may be eliminated by taking the logarithmic derivatives of Eqs. (3) and (4) and combining to obtain:

$$t_+ = \frac{-\frac{\gamma+1}{4\gamma c} r \frac{\Delta P}{P(r)}}{\left[1 + \frac{r}{2} \frac{\partial}{\partial r} \ln P(r) + r \frac{\partial}{\partial r} \ln \frac{\Delta P}{P(r)}\right]} \tag{5}$$

For an exponential atmosphere this becomes:

$$t_+ = \frac{-\frac{\gamma+1}{4\gamma c} r \frac{\Delta P}{P}}{\left[1 - \frac{r}{2H} + n\right]} \quad , \tag{6}$$

where

$$n \equiv r \frac{\partial}{\partial r} \ell n \frac{\Delta P}{P} \, . \tag{7}$$

The value of n is obtained from Eq. (1):

$$n(r) \equiv r \frac{\partial}{\partial r} \ell n \frac{\Delta P}{P} = \left[1 - \frac{r}{3H}\right] \left(\frac{P_b}{\gamma}\right)^{1/3} r \frac{f'}{f}$$

$$= \left[1 - \frac{r}{3H}\right] n_h \quad , \tag{8}$$

where f' is the derivative of f with respect to its argument and n_h is the value of n for a homogeneous atmosphere ($H \to \infty$). The quantity n_h is plotted vs. relative overpressure in Fig. 3. Note that, consistent with Figure 2, the minimum value of $\frac{\Delta P}{P}$ corresponding to n = 0 occurs at r = 3H, that is at an altitude 3 scale heights above the burst point.

Combining Eqs. (6) - (8) we obtain:

$$t_+ = \frac{-\frac{\gamma+1}{4\gamma c} r \frac{\Delta P}{P}}{(1 + n_h) - \frac{r}{2h}\left(1 + \frac{2}{3} n_h\right)} \tag{9}$$

At $r = r_o$, $\frac{\Delta P_o}{P_o} = .2$, and according to Figure 3, $n_h = -\frac{3}{2}$. Thus we obtain from Eq. (9):

$$t_+^o = \frac{\gamma+1}{\gamma c} (.1) \, r_o, \tag{10}$$

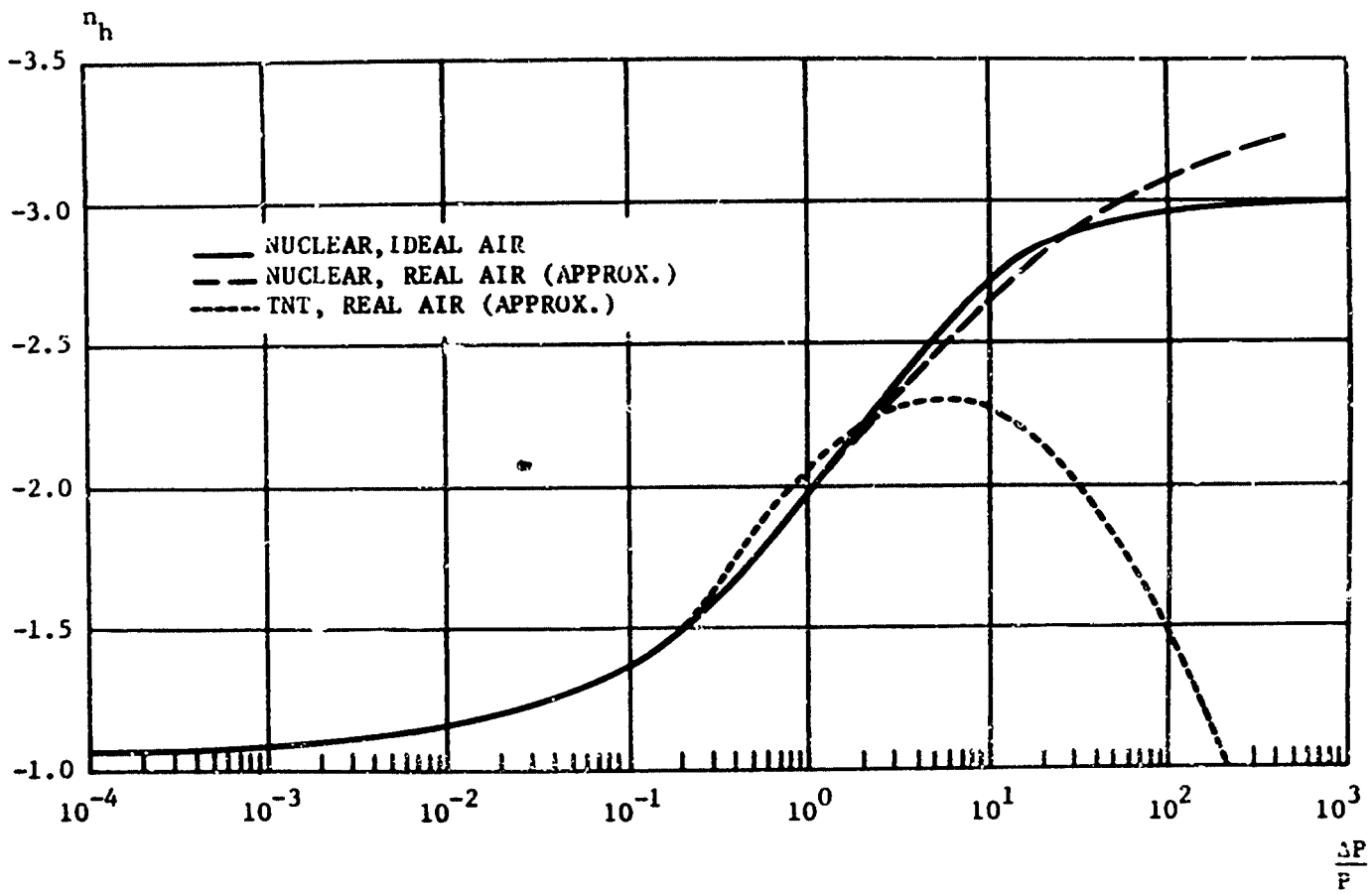

FIGURE 3. The Parameter n_h vs Relative Overpressure. From LEHTO and LARSON (1969).

which permits Eqs. (3) and (4) to be written as:

$$t_+ = \frac{\gamma+1}{\gamma c}(.1)\, r_o \left[1 + e^{-r_o/2H}\left[E_i\left(\frac{r}{2H}\right) - E_i\left(\frac{r_o}{2H}\right)\right]\right]^{\frac{1}{2}} \tag{11}$$

$$\frac{\Delta P}{P} = \frac{.2\,\frac{r_o}{r}\, e^{-(r_o-r)/2H}}{\left\{1 + e^{-r_o/2H}\left[E_i\left(\frac{r}{2H}\right) - E_i\left(\frac{r_o}{2H}\right)\right]\right\}^{\frac{1}{2}}}\ , \tag{12}$$

where r_o is given by Eq. (2) and where the exponential integral E_i is defined as:

$$E_i(x) = \int_{-\infty}^{x} \frac{e^t}{t}\, dt\ . \tag{13}$$

At the base of the ionosphere (considering only low altitude detonations) the term $e^{-r_o/2H} E_i\left(\frac{r}{2H}\right)$ dominates in the radicals occurring in Eqs. (11) and (12) and furthermore may be approximated as $\frac{2H}{r} \exp\left[\frac{r-r_o}{2H}\right]$.

Making this approximation and using Eq. (2) to eliminate factors of $r_o\, e^{-r_o/3H}$ we obtain from Eqs. (11) and (12):

$$t_+ = .075\, \frac{\gamma+1}{\gamma c} \left(\frac{\gamma}{P_b}\right)^{1/3} e^{r_o/12H} \sqrt{\frac{H}{r}}\ e^{r/4H} \tag{14}$$

$$\frac{\Delta P}{P} = .075 \left(\frac{\gamma}{P_b}\right)^{1/3} e^{r_o/12H}\ \frac{e^{r/4H}}{\sqrt{Hr}} \tag{15}$$

The factor $e^{r_o/12H}$ may be neglected since r_o cannot be larger than 3H, the reason being that $\frac{\Delta P}{P} = .2$ must occur before the minimum at $r_o = 3H$ if it is to occur at all. (According to Eq. (2), $\frac{\Delta P}{P}$ does not become as small as .2 for sea level yields in excess of 60 MT.) We set $\frac{r}{H} = \frac{z-z_b}{H_s}$, where z is the shock altitude, z_b is the burst altitude ($e^{-z_b/H_s} = P_b$), and H_s is the scale height in the vertical direction. Then taking H_s = 7 km, γ = 1.4, and c = .31 km/sec as representative values below 120 km altitude we obtain the final form of our expressions for the shock positive phase duration and relative overpressure:

$$t_+ = 1.1\ Y^{1/3}\ P_b^{-1/12}\ \frac{e^{z/28}}{\sqrt{z - z_b}} \tag{16}$$

$$\frac{\Delta P}{P} = .028\ Y^{1/3}\ P_b^{-1/12}\ \frac{\sqrt{z - z_b}}{r}\ e^{z/28} \tag{17}$$

For 4MT at 5 km and for shock propagation at 45° from the horizontal Eq. (17) predicts $\frac{\Delta P}{P}$ = 1.2 at 100 km altitude. The SAP and SHELL results shown in Figure 1 both give about $\frac{\Delta P}{P}$ = 1.6 at this altitude. That the agreement is only approximate is not surprising in view of the several assumptions made and in particular due to the fact that the weak shock theory employed becomes inaccurate when $\frac{\Delta P}{P} \gtrsim 1$. For smaller yields or propagation closer to the horizontal the theoretical results should be more accurate.

The properties of the shock when it reaches the ionospheric level are given by Eqs. (16) and (17). These properties, which will be used in the subsequent discussion, are as follows:

a. The relative overpressure and positive phase duration are both proportional to cube root of yield.

b. Both relative overpressure and positive phase duration are insensitive to height of burst at least for low altitude

detonations. Taking z to be 100 km and recalling that $P_b \sim e^{-z_b/H}$ where H is taken to be 7 km we find that the respective height of burst dependences are: $t_+ \sim \left[1 + z_b/59\right]$ and $\Delta P/P \sim \left[1 + z_b/145\right]$, where z_b is in kilometers.

c. For a given altitude the positive phase duration is independent of range and the relative overpressure decreases linearly with range.

d. A megaton detonation at sea level has a positive phase duration of about 39 seconds at 100 km.

3.2.2 Direct Effects of the Shock

We believe the direct effects of the shock to be the source of the many observations of ionospheric disturbances following nuclear tests with periods between 30 seconds and 10 minutes, periods of about a minute being predominant (BAKER, D. M., 1968). These disturbances were observed by a doppler technique between altitudes of 150 and 200 km and appeared to propagate at speeds of about 300 meters/sec. Typically the explosions involved were the order of a megaton.

An example is shown in Figure 4 of the disturbance observed following the United States megaton range detonation Housatonic on 30 October 1962 (GLASSTONE, S., 1964, pg. 677e). BAKER (1968) points out that a feature occurs on 4 MHz, which is reflected from 180 km, about 17 seconds earlier than a 5 MHz, which is reflected from 190 km. He finds therefore that the disturbance was propagating upward with a speed approximately equal to the local sound speed. On this basis and because of the known acoustic ducting properties of the atmosphere he hypothesizes that the acoustic signal has the bulk of its energy confined in a duct below 110-120 km altitude and that it is leakage from this duct that is responsible for the ionospheric disturbance.

The point we wish to make is that the observed periods of these ionospheric disturbances are approximately the same as the periods which the shock from a megaton range explosion would contain on reaching the ionospheric level. We say approximately because among other things it is not clear whether the periods contained in the shock are the order of $2t_+$ or some slightly larger value. In terms of Figure 1

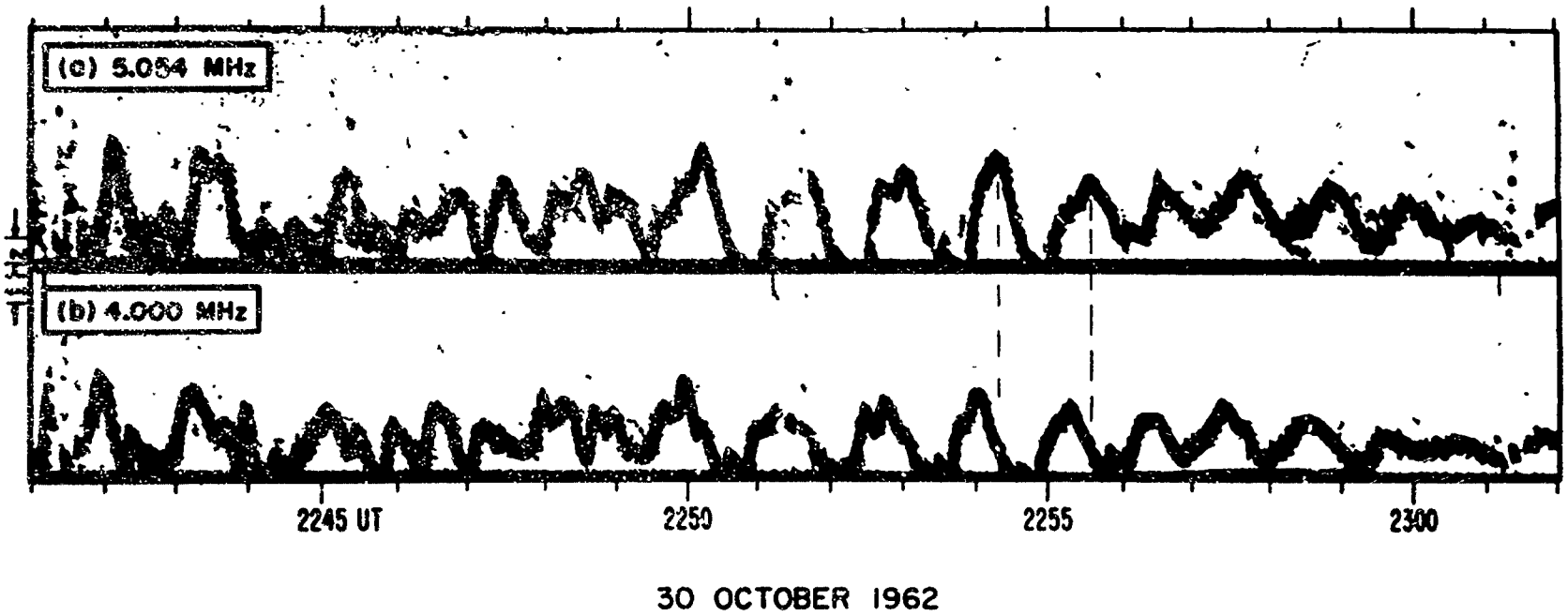

FIGURE 4. Detail of Ionospheric Disturbance Above Boulder on October 30, 1962. From BAKER (1968).

this means that the portion of the shock which initially propagates at angles of from about 20^{o} to 35^{o} is responsible for these short period ionospheric disturbances.

Ionospheric disturbances with periods greater than 10 minutes, which we now discuss, are related in a complex manner to the portions of the shock which initially propagate at steeper angles to the horizontal.

3.2.3 Long Period Acoustic-Gravity Wave Generation by the Upward Going Shock

As previously noted, Figure 2 shows a dramatic drop in relative overpressure commencing at about the 100 km altitude level. The reason for this can be seen by examining the SHELL outputs for the detailed flow, one of which is shown in Figure 5. This Figure is a contour plot of relative pressure as a function of altitude and horizontal distance at a time of 600 seconds. The spherically expanding and upward moving shock wave is refracted at the 100-120 km altitude level where the ambient temperature beings to increase radically. Of course, the vertically propagating shock front is unrefracted. The result is the generation of a horizontally propagating disturbance in the flow behind the shock front. This disturbance drains energy from the shock which continues outward and upward.

The essential feature of the Greene-Whitaker calculation is that the effective source of the long period gravity wave disturbance is located at an altitude of 100-120 km above the burst. The effective source commences 10 minutes or more after a sea level detonation, this being the time required for the shock wave to reach the ionospheric level and for the rotating flow of Figure 3 to become established. This delay time correction to the travel time has been observed following several low altitude explosions (HERRON, T.J., 1971).

The velocity vector plots, which are not shown, indicate that the dominant motion in the disturbance depicted in Figure 5 is a rotating or vortex flow and on this basis we proceed to estimate the disturbance kinetic energy. The geometry assumed for this vortex flow is indicated in Figure 6.

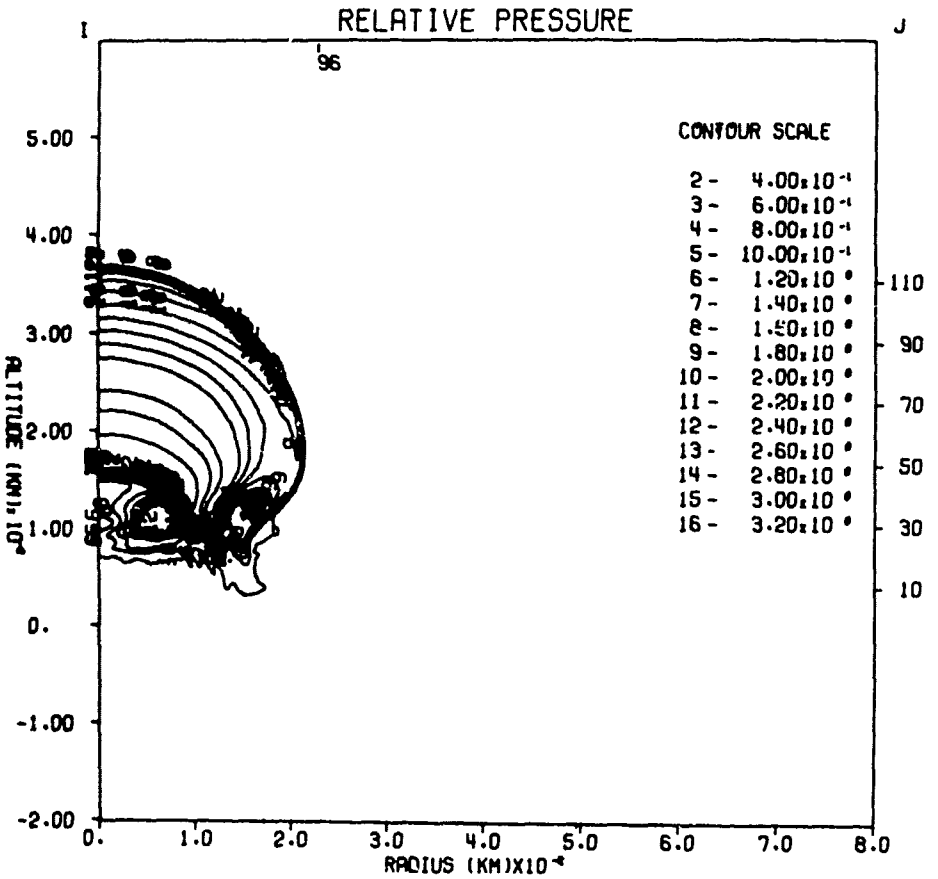

FIGURE 5. SHELL Calculation of 4 MT Isothermal Sphere at a Time of 600 Seconds Showing Contours of Relative Pressure. From GREENE and WHITAKER (1968).

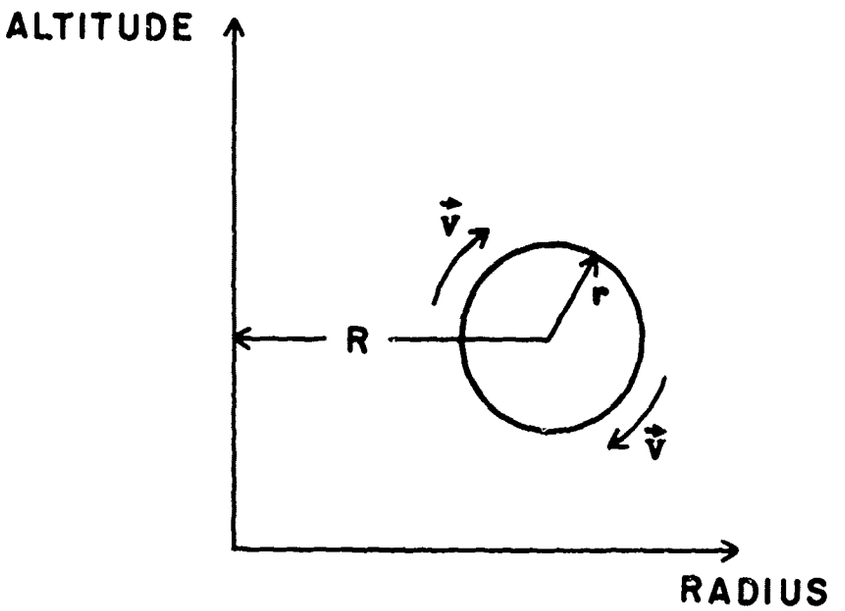

FIGURE 6. Assumed Geometry for Vortical Flow Due to the Greene-Whitaker Mechanism.

The kinetic energy of the motion is:

$$E_s = \int \tfrac{1}{2} \rho \, v^2 \, dV, \tag{18}$$

where the volume element for the region containing the vortical flow is:

$$dV = 2 \pi R \, (2\pi r' \, dr') \tag{19}$$

For the assumed flow we may define a constant vorticity within the rotating region:

$$\omega = \tfrac{1}{2} \, |\nabla \times \vec{v}| = \frac{v(r')}{2r'} \tag{20}$$

in terms of which Eq. (18) becomes:

$$E_s = 8 \, \pi^2 \omega^2 \, R \int_0^r \rho(r') \, r'^3 \, dr', \tag{21}$$

and approximating $\rho(r')$ by ρ_a, the ambient density, this results in:

$$E_s = 2 \, \pi^2 \, \omega^2 \, r^4 \, R \, \rho_a \tag{22}$$

We estimate R = 150 km and r ≈ 30 km based on Figure 5. This latter value is approximately the gradient scale of the temperature change responsible for the shock refraction and development of the vortical motion, i.e. T/∇T ≈ r. We estimate the maximum flow velocity v(r) as being approximately equal to the sound speed at 130 km, that is about .64 km/sec. Then for an ambient density of 7.6×10^{-9} kg/meter^3 we obtain E = 5 KT, that is about .1% of the total 4 MT yield.

For smaller yields than our 4 MT example, the yield scaling of kinetic energy in the horizontally propagating disturbance is easily obtained. The kinetic energy is $\tfrac{1}{2} \rho v^2 V$, where ρ is the density, v the fluid velocity, and V the volume over which the rotational motion takes place. For a weak shock we expect only the fluid velocity to be a

function of the detonation parameters. Since this velocity is proportional to the relative overpressure we find from Eq. (17) that the energy in the horizontally propagating disturbance is proportional to $Y^{2/3}$. Thus with a proportionality constant determined by the 4MT example we may write:

$$E_{s/Y} \approx 2 \times 10^{-2} Y^{1/3}. \tag{23}$$

We will compare this estimate with the energy available in the rising fireball for wave generation, which is derived below.

3.3 FIREBALL GENERATION OF ACOUSTIC-GRAVITY WAVES

The fireball is a buoyant rising fluid element and as such deforms into a torus or vortex ring configuration. The flow is illustrated in Figure 7. During the initial rise period, that is, well before the stabilization time the flow around this vortex ring can be treated as the flow around an equivalent solid object. Warren (1960) has calculated the wave emission and wave drag on a sphere moving vertically in a stratified incompressible fluid. His theory predicts that gravity wave emission is negligible when

$$\frac{\Omega}{N} > 1, \tag{24}$$

where $\Omega = v/2a$, v is the sphere velocity, and a the sphere radius. The Brunt-Väisälä frequency N, is the high frequency cutoff for gravity wave propagation. The onset of wave emission at $\Omega/N \approx 1$ has been experimentally verified (MOWBRAY, D. E. and B. S. H. Rarity, 1967).

A buoyant sphere rises at a velocity (SCORER, R. D., 1950)

$$v \approx (g \beta a)^{\frac{1}{2}}, \tag{25}$$

where g is the acceleration of gravity and $\beta \approx \frac{\rho - \rho'}{\rho}$ is the buoyancy defined as the difference in density between the fireball and its surroundings divided by the ambient density.

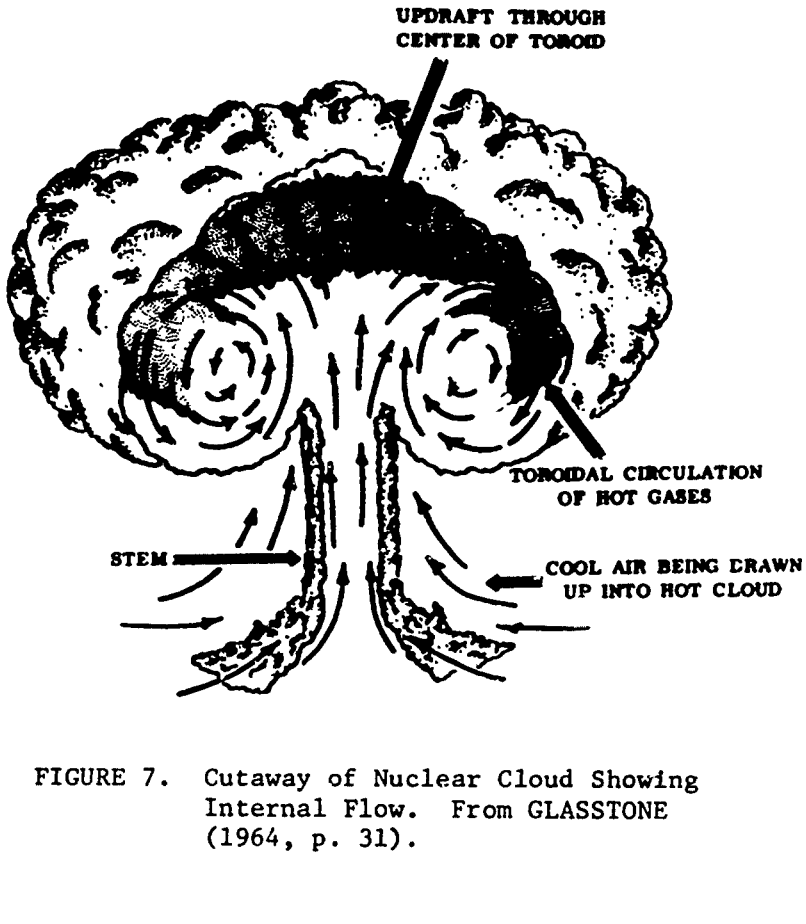

FIGURE 7. Cutaway of Nuclear Cloud Showing Internal Flow. From GLASSTONE (1964, p. 31).

Warren's criterion for significant gravity wave emission therefore gives:

$$a > g\,\beta \left(\frac{\tau_{Bv}}{4\pi}\right)^2 \tag{26}$$

$$\approx 5.6\,\beta \text{ km},$$

for a Brunt-Väisälä period τ_{Bv} of 5 minutes. Because of the very high fireball temperatures involved at early times we may approximate β by unity. Then Eq. (26) states that a fireball radius of 5.6 km is required for the onset of appreciable gravity wave emission. According to the data in Glasstone (1964,p 10) this would require a yield in excess of 30MT. We conclude that for sea level detonations only very large yields could result in gravity wave emission during the initial period of the rise.

When the fireball reaches its stabilization altitude and proceeds toward hydrodynamic equilibrium with its surroundings, conditions more favorable for gravity wave emission do occur. However, before considering the details of how this wave emission arises we conclude our discussion of the initial rise period by computing the fraction of the total yield which is contained in the kinetic energy of the rising fireball for a sea level detonation. We wish to compare this energy with our previous estimate for the energy available in the shock for long period gravity wave generation. The fireball kinetic energy is:

$$E_f = \tfrac{1}{2}\,Mv^2 = \tfrac{1}{2}\,M\,g\,\beta\,a \tag{27}$$

where we have used Eq. (25) for V. The mass occurring in Eq. (27) is not the mass of the fireball itself but rather that of the considerably larger mass of ambient air which moves with the fireball, the so called virtual mass (DARWIN, 1953). This mass is equal to half the mass of ambient air which would occupy the fireball volume. Accordingly we write:

$$E_f = \frac{\pi}{3}\,a^4\,\rho\,g\,\beta \tag{28}$$

According to Glasstone (1964, pp. 74 - 75) the terminal fireball radius is about 750 feet for a 20 KT detonation. The temperature at the time (1 sec) this radius is achieved is about 10 times ambient, and hence assuming pressure equilibrium $\beta = .9$. Assuming cube root scaling with yield we may then write, $a = 8.45 \times 10^3 Y^{1/3}$cm, where Y is in kilotons. Eq. (28) then gives the fraction of the yield which is available as kinetic energy of fireball rise:

$$\frac{E_f}{Y} = 1.5 \times 10^{-4} Y^{1/3} \tag{29}$$

Comparing this with Eq. (23) we find that for a yield of about 1.6 MT $E_f = E_s$. Thus for yields in excess of this value we expect the energy available in the rising fireball for long period gravity wave generation to be greater than the similar energy available in the upward going shock.

We now turn to a description of how this fireball rise energy becomes available for the generation of long period gravity waves.

3.3.1 Oscillating Vortex Model of Fireball Stabilization

In this section, the relation between a fireball in the terminal phase of its motion and the fluid oscillations that result as it stops rising are considered. An approximate expression for the frequency of the resulting motion is derived in terms of the final motions of the fireball and the atmospheric parameters. Our analysis of gravity wave generation by a rising fireball differs from the work of Tolstoy and Lau (1971) in that it is based on the theory of buoyant vortex rings.

We consider a ring vortex where the core radius R_o is much smaller than the major radius R as shown in Figure 8. The substance, a spheroidal mass of air surrounding the ring, moves with the ring. The difference between the mass contained in the ring and in the substance and an equal volume of the atmosphere is:

$$\Delta M = 2\pi \int_0^{\bar{r}} \int_{z_1(r)}^{z_2(r)} (\rho' - \rho_o)\, dz\, r dr, \tag{30}$$

where $\rho'(r,z)$ is the mass density inside the vortex, $\rho_o(z)$ is the ambient density, and $z_2(r)$, $z_1(r)$ define the boundaries of the substance.

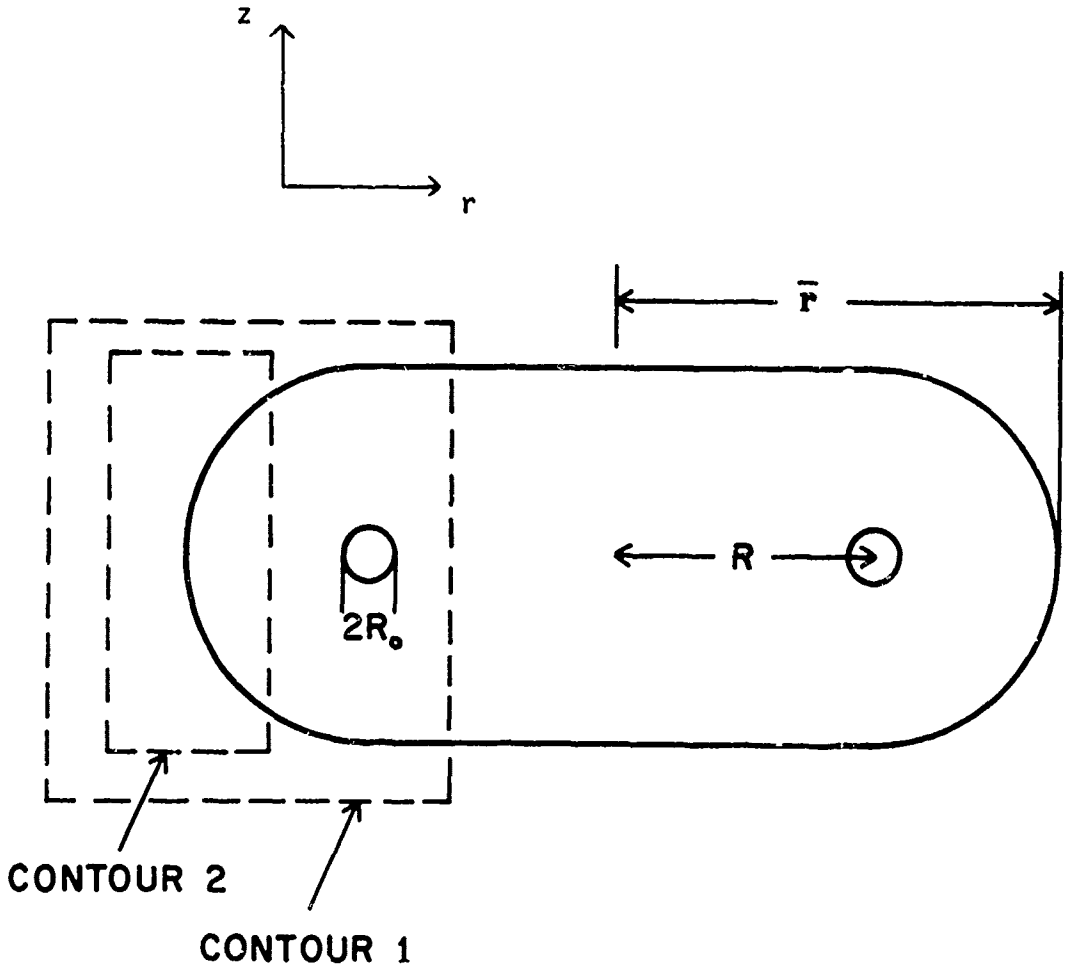

FIGURE 8. Assumed Vortex Ring Configuration with Contours Used to Calculate Vorticity.

On a contour such as 1, which contains but does not intersect the core, the circulation K is given by:

$$K = \frac{R\dot{\ell}}{C} , \tag{31}$$

where the dot indicates a time derivative. The quantity C depends logarithmically on the distribution of vorticity within the ring. We assume that the motion is similar and that therefore C is a constant.

The circulation along contours such as 1 and 2 changes during the rise according to the Bjerkness Eq:

$$\dot{K} = - \oint \frac{dp}{\rho} , \tag{32}$$

where p is the pressure, taken to be ambient under the assumption that equilibrium has been obtained.

On a contour such as 2 which does not contain the core, K = 0 at all times and hence $\dot{K} = 0$ at all times. On any contour such as 1, which contains but does not intersect the core, K must be the same. Hence at any time $\dot{K}$ must be the same for all such contours.

Eq. (32) can be rewritten:

$$\dot{K} = -\oint \frac{dp}{\rho} = - \oint \frac{dp}{\rho_o} - \int_{z_1(r)}^{z_2(r)} \frac{dp}{\rho'} + \int_{z_1(r)}^{z_2(r)} \frac{dp}{\rho_o} \tag{33}$$

$$= - \int_{z_1}^{\dot{z}_2} dp \; \frac{(\rho_o - \rho')}{\rho' \rho_o}$$

since $\oint \frac{dp}{\rho_o} = 0$. Using the hydrostatic equilibrium equation $\frac{dp}{dz} = - g\rho_o$ Eq. (33) finally, becomes:

$$\dot{K} = g \int_{z_1(r)}^{z_2(r)} \frac{\rho_o - \rho'}{\rho'} \, dz \tag{34}$$

which is nonzero and independent of r for $r \leq R - R_o$ and is zero for $r \geq R + R_o$. Since the model is intended to apply to the later stages of fireball rise when the buoyancy has become small we replace ρ' in the denominator of Eq. (34) by ρ_o. We further assume that the fireball is small enough that the integration in Eq. (34) takes place over much less than an atmospheric scale height and that the factor $1/\rho_o$ may be taken outside the integral. Then using Eq. (34) we may rewrite Eq. (30) as:

$$\Delta M = -\frac{2\pi}{g}\rho_o \int_o^{\bar{r}} \dot{K} \quad r dr \tag{35}$$

$$= -\frac{\dot{K}\pi}{g}\rho_o \quad (R^2 - R_o^2) \quad \simeq -\frac{\pi R^2}{g} \quad \rho_o \dot{K}$$

Conservation of mass gives:

$$\frac{d}{dt}\rho'' V = \rho_o \left(\frac{dV}{dt} - \frac{dV_a}{dt}\right), \tag{36}$$

where V is the volume over which the integration in Eq. (30) is done and ρ'' is the average density within this volume. The term dV_a/dt represents the volume change due to adiabatic expansion as the vortex moves upwards:

$$\frac{dV_a}{dt} = -\frac{1}{\gamma} V \frac{1}{\rho_o} \frac{d\rho_o}{dt} \tag{37}$$

Thus Eq. (36) becomes:

$$\frac{d}{dt} \quad V \ (\rho'' - \rho_o) = \frac{d\Delta M}{dt} \quad = -V \frac{\gamma - 1}{\gamma} \quad \frac{d\rho_o}{dt} \tag{38}$$

combining this result with Eq. (35) for ΔM we obtain

$$\ddot{K} + \dot{K} \frac{d}{dt} \ln \rho_o R^2 - \frac{gV}{\pi R^2} \frac{\gamma - 1}{\gamma} \frac{1}{\rho_o} \frac{d\rho_o}{dt} = 0 \qquad (39)$$

making use of the fact that

$\frac{d\rho_o}{dt} = \frac{\partial \rho_o}{\partial z} \dot{z}$ and $\dot{z} = C \frac{K}{R}$ this becomes:

$$\ddot{K} + \dot{K} \frac{d}{dt} \ln \rho R^2 + \alpha^2 N^2 K = 0 \qquad (40)$$

where $N^2 = - \frac{(\gamma - 1)}{\gamma} \frac{g}{\rho_o} \frac{\partial \rho_o}{\partial z}$ is the ambient Brunt Väisälä frequency and $\alpha^2 = \frac{CV}{\pi R^3}$ is a constant of order unity as discussed below. Eq. (40) is most conveniently solved in terms of an auxilliary function Q:

$$K = \frac{Q}{\sqrt{\rho_o} R} \qquad (41)$$

where:

$$\ddot{Q} + \left[\alpha^2 N^2 - \frac{\left| \sqrt{\rho_o} \ddot{R} \right|}{\sqrt{\rho_o} R} \right] Q = 0 \qquad (42)$$

and where $(\sqrt{\rho_o} \ddot{R})$ represents $\frac{d^2}{dt^2} (\sqrt{\rho_o} R)$.

Assuming that the bracketed term in Eq. (42) is slowly varying we obtain the WKB solution:

$$Q \sim \frac{\exp i \int \left[\alpha^2 N^2 - \frac{(\sqrt{\rho_o}\,\ddot{R})}{\sqrt{\rho_o}\,R}\right]^{\frac{1}{2}} dt}{\left[\alpha^2 N^2 - \frac{(\sqrt{\rho_o}\,\ddot{R})}{\sqrt{\rho_o}\,R}\right]^{\frac{1}{4}}} \qquad (43)$$

Using Eqs. (31) and (41) this gives the solution for $\dot{z}$:

$$\dot{z} \sim \frac{1}{\sqrt{\rho_o}\,R^2} \frac{\exp i \int \left[\alpha^2 N^2 - \frac{(\sqrt{\rho_o}\,\ddot{R})}{\sqrt{\rho_o}\,R}\right]^{\frac{1}{2}} dt}{\left[\alpha^2 N^2 - \frac{(\sqrt{\rho_o}\,\ddot{R})}{\sqrt{\rho_o}\,R}\right]^{\frac{1}{4}}} \qquad (44)$$

Before discussing the physical significance of this equation it is useful to consider the quantity $\alpha = \frac{CV}{\pi R^3}$ in more detail. The volume V is approximately equal $\pi R^2 \Delta z$, where Δz is the vertical distance over which the z integration in Eq. (30) is done. Alternatively Δz may be interpreted as the effective distance beneath the ring from which fluid is drawn up to the ring. Observations of laboratory releases of buoyant fluid with a spheroidal substance suggest the value $\Delta z \approx 3R$ (TURNER, J. S., 1960). The quantity C is about .13 for a spherical vortex (LAMB, 1932). This gives $\alpha \approx .62$. In general we expect α to be constant so long as C is, and to have a value somewhat less than unity.

Equation (44) applies from the time the fireball has formed a vortex ring and has entrained sufficient air that the interior density ρ' is approximately equal to the ambient value ρ_o. Thus we are not able to describe the early stages of the rise. However, the more time consuming later stages of the rise will occur on a time scale the order of $\frac{\pi}{\alpha N}$, that is on the order of the Brunt-Väisälä period. For nuclear clouds which do not spread rapidly when approaching their stabilization altitude, vertical oscillations will occur at a frequency αN. According to Eq. (44), clouds which spread rapidly will undergo oscillations at a lower frequency than αN and the amplitude of the oscillations will subside as $1/R^2$ as the cloud

spreads. If the cloud radius spreads sufficiently rapidly (such as exponentially on a time scale shorter than τ_{BV}) there will be no oscillatory motion and the approach to equilibrum will be overdamped.

In any case, for megaton range detonations where the nuclear cloud penetrates into the very stable stratosphere, a rapid growth in cloud radius ensues (GLASSTONE 1964, pp. 35-37). This would tend to reduce the amplitude of gravity waves due to vertical oscillations of the cloud. In general, for given atmospheric conditions there may be an optimum yield-height of burst combination for gravity wave generation by the stabilized fireball but it is currently unknown.

To gain further insight into the wave pattern generated by this type of buoyant oscillation, laboratory experiments have been performed at Mt. Auburn, as described below.

3.3.2 Laboratory Observations of Gravity Wave Generation by Buoyantly Rising Masses

A photograph of the experimental apparatus is shown in Figure 9. The experiments were performed in a plexiglas tank 5' x 3' x 3½' deep. A linearly stratified density fluid (salt and water) was established in the tank by carefully introducing fluid layers of successively decreasing density. This stratification very closely approximates an exponential medium over the dimensions of the experimental region. The density gradient was checked by carefully weighing a 300 cc teflon rod suspended at varying depths in the fluid, and after some days it was found that the initial density discontinuities had smoothed out to form a linear density gradient. Using ethyl alcohol as the buoyant, miscible fluid, a number of buoyant releases were made from a release mechanism on the base surface of the tank. Visualization of the wave motions in the fluid was achieved using small neutrally buoyant polystyrene beads which acted as excellent scattering centers for a well collimated light beam. Thus a cross-section through the fluid motions was observed.

A 16 mm cine camera was used to record the internal wave motions and a schematic drawing based on a sample frame is shown in Figure 10. For this release the buoyant fluid was dyed to be readily observable. The formation of a vortex ring structure and vertical oscillations and rapid spreading of the initially buoyant fluid as it reached its equilibrium level were clearly observed.

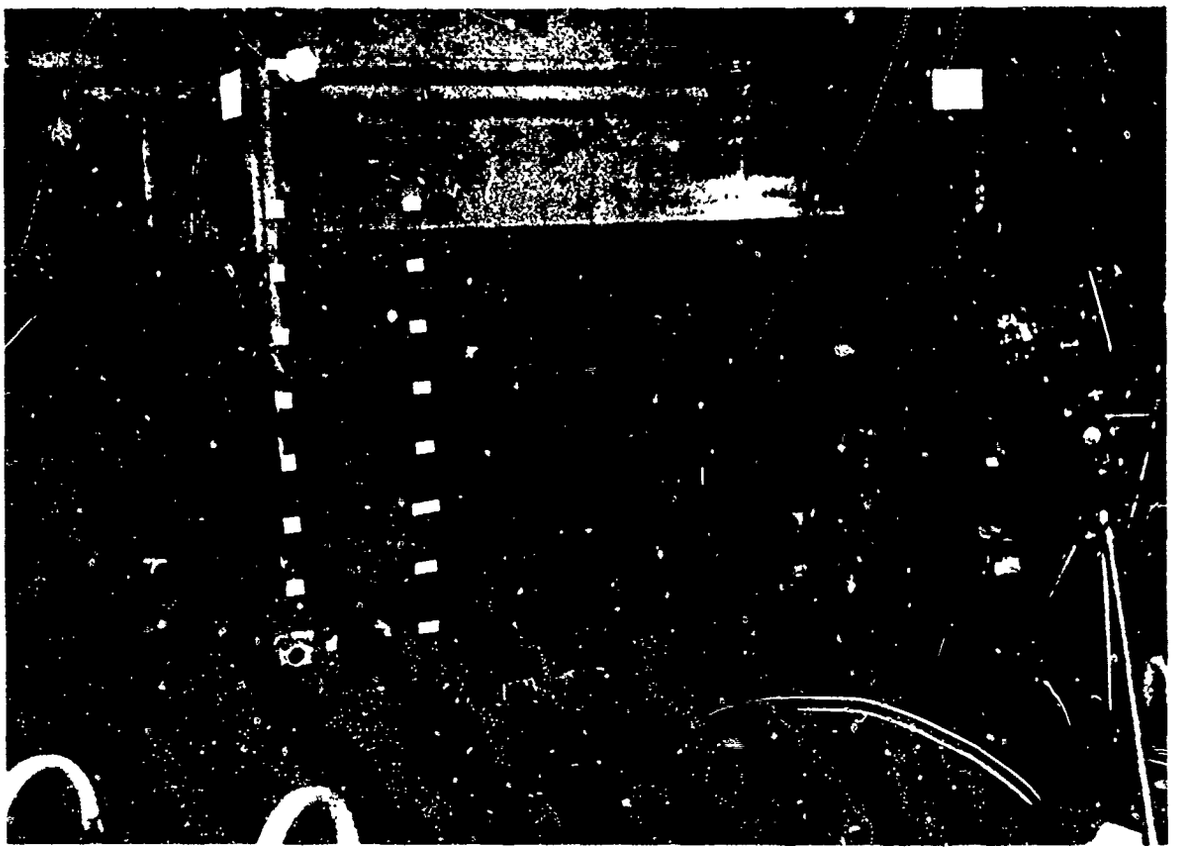

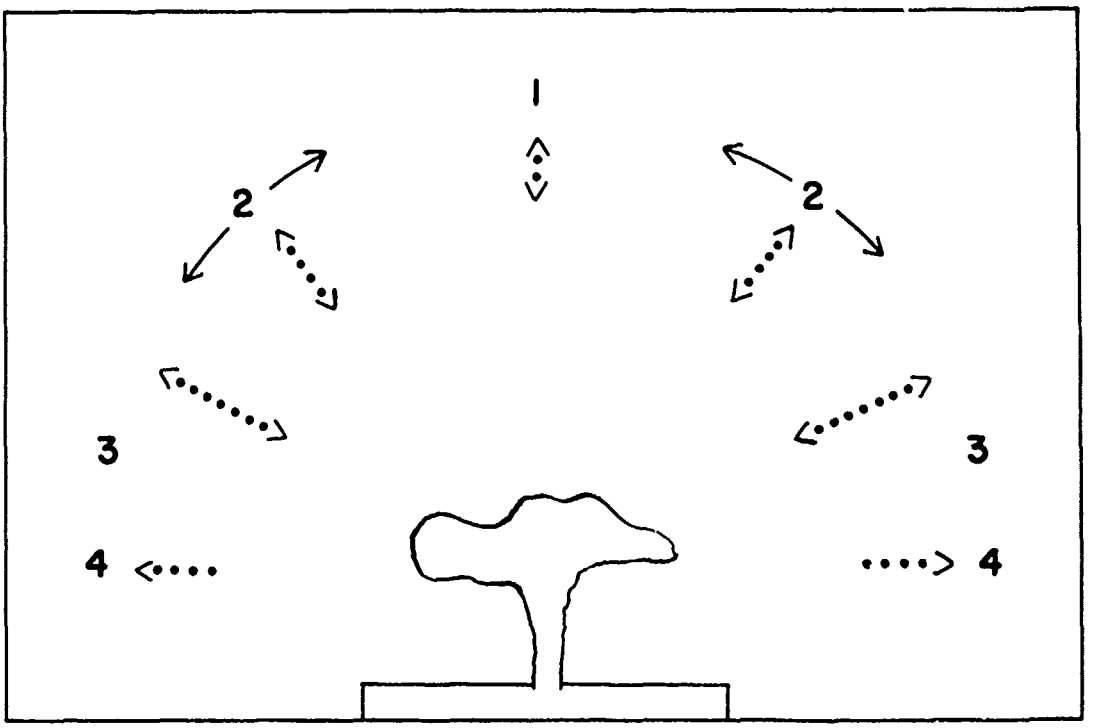

FIGURE 10. Observed Wave Pattern Showing Angular Regions Described in Text.

Typically the time required for the top of the released fluid to reach its maximum altitude was about 8 seconds, somewhat shorter than the Brunt-Väisälä period in the tank (9.8 seconds).

The wave pattern, which was more complex than anticipated, is conveniently divided into the four regions shown in Figure 10: (1) Directly above and below the source region small amplitude oscillations of the beads were observed. The period of these oscillations as nearly as could be determined was equal to the Brunt-Väisälä period. (2) The amplitude and the period of the oscillations increased with increasing angle from the vertical. The amplitude reached a maximum at an angle of about 60^{o} where the period was about 12 seconds. (3) The amplitude then decreased slightly with increasing angle. This region existed over a relatively small angle and it was difficult to observe changes in the period within this region. (4) Finally, at very small angles to the horizontal planes of stratification, motion of the beads was observed which was not periodic, rather the beads were displaced away from the source region and did not return. This motion is clearly related to the horizontal spreading of the initially buoyant fluid as it equilibrates.

The propagation theory for acoustic-gravity waves predicts that waves of period τ whose vertical wavelength is less than a scale height should propagate at an angle θ from the vertical (HINES, C.O., 1960), where:

$$\frac{\tau_{BV}}{\tau} = |\cos \theta| \qquad (45)$$

This propagation law does appear to be obeyed in the experiment since $\tau \simeq \tau_{BV}$ at $\theta = 0, \pi$ and $\tau \simeq \frac{2}{\sqrt{3}} \tau_{BV}$ at $\theta = \pi/3, 2\pi/3$. In theory there should be no propagating solution exactly at $\theta = 0, \pi$ where $\tau \simeq \tau_{BV}$. However, because the characteristic wavelengths in the experiment are much larger than the dimensions of the tank we are unable to distinguish propagating from spatially damped disturbances.

Perhaps the most interesting aspect of the laboratory observations is the confirmation of the theoretical prediction that much of the

buoyant rise energy is utilized to generate waves in the period range $1 - 2\ \tau_{BV}$. Our expectation is that an analogous process of wave generation would occur for a stabilizing nuclear cloud. However, while we are able to estimate the period of the largest amplitude portion of the disturbance we have not estimated what fraction of the available energy goes into very long periods, that is periods many times the Brunt-Väisälä period. These long period waves would propagate at shallow angles to the horizontal and it may be that atmospheric refraction would prevent their reaching ionospheric levels. In this connection it is interesting to note that ionospheric disturbances of about 3 minutes period, which are associated with severe weather, are not normally observed more than 250 km horizontally from the apparent source location (GEORGES, T. M., 1968). Whether the absence of longer periods at greater horizontal distances is a result of properties of the source or of atmospheric filtering and refraction is not known.

3.4 CONCLUSIONS

In the preceding sections we have attempted to relate the different kinds of disturbance seen in the ionosphere to the hydrodynamic motions accompanying a low altitude nuclear explosion. The short period ionospheric disturbances seem to be caused by the portion of the shock front which is reflected from the 100-120 km altitude level. This identification is made because the periods contained within the shock when it reaches this altitude level are the order of the observed ionospheric periods, that is, about a minute. We expect the ionospheric periods to scale with explosion parameters in the same way as does the shock positive phase duration at the 100-120 km altitude level. The ionospheric periods should therefore be proportional to the cube root of yield and essentially independent of height of burst.

The origin of ionospheric disturbances with periods exceeding 10 minutes is a more complex problem since both the upward going shock and the rising fireball are possible hydrodynamic sources. For yields in excess of about a megaton the energy available in fireball rise for the production of long period disturbances exceeds that available in the upward going shock.

The mechanism described by Greene and Whitaker (1968) for the generation of long period ionospheric waves involves a refraction of the upward going shock at the 100-120 km altitude level. This results in a transfer of energy from the shock to a horizontally propagating disturbance which is left behind. The Greene-Whitaker mechanism is generally operative since conditions for this shock refraction are a permanent feature of the atmosphere.

The fireball is most efficient in the generation of long period acoustic-gravity waves when it has reached its terminal altitude and is approaching hydrodynamic equilibrium with the atmosphere. It may then undergo vertical oscillations with a period somewhat larger than the Brunt-Väisälä period. The efficiency of wave generation by this mechanism is very sensitive to ambient conditions at the tropopause as well as to burst parameters. In particular nuclear clouds which undergo rapid spreading upon stabilization appear to be inefficient wave generators. In theory, and this is supported by laboratory experiments, the terminal phases of fireball rise, when the mechanism is efficient, produce a wave spectrum with amplitudes peaked at one to two times the Brunt-Väisälä period. These periods propagate at relatively steep angles to the horizontal and would primarily affect the ionosphere near the burst. Whether significant wave amplitudes could be produced at much longer periods is presently unknown as is the question of whether these long periods, which propagate at shallow angles to the horizontal, would be prevented by atmospheric refraction from reaching ionospheric levels.

4. EXPERIMENTAL INVESTIGATION OF INTERNAL WAVES GENERATED BY A BUOYANTLY RISING FLUID

4.1 INTRODUCTION

There has been considerable interest in the generation and propagation of waves in the atmospheres of earth and other planets, and a number of authors (LAMB, 1945; ECKART, 1960; TOLSTOY, 1963; PIERCE, 1966) have discussed the mathematical formulation of the relevant wave equations. Experimental investigations have also been carried by MOWBRAY and RARITY, 1967; WU, 1969; HURLEY, 1969; SCHOOLEY and HUGHES, 1972.

The present work is the first experimental investigation of the internal gravity wavefield generated by the motion of a buoyantly rising fluid in an incompressible, density-stratified atmosphere. Also for the first time the trajectories of specific fluid elements in the wavefield have been observed and the results appear to be in close accord with theoretical predictions.

4.2 EXPERIMENTAL FACILITY AND TECHNIQUE

4.2.1 Description of Apparatus

Figure 1 shows a photograph of the main experimental facility, a plexiglas tank of dimensions 5' x 3' x 3½' deep. This tank contains the stratified fluid, which in our experiments was a solution of varying amounts of salt in water. Distilled water was used to improve the light transmission characteristics of the solution. The procedure for filling the tank with the density-stratified solution was as follows: first a solution with the maximum density of salt was filled into the tank, typically to a depth of 3 or 4 inches. Next a similar volume of somewhat lower density solution was floated on top of the first. This was achieved by flowing the new solution onto a thin board floating on the top surface of the liquid already in the tank so as to minimize vertical mixing. Using this technique, adjacent fluid strata with density differences of less than 5×10^{-3} could be clearly established.

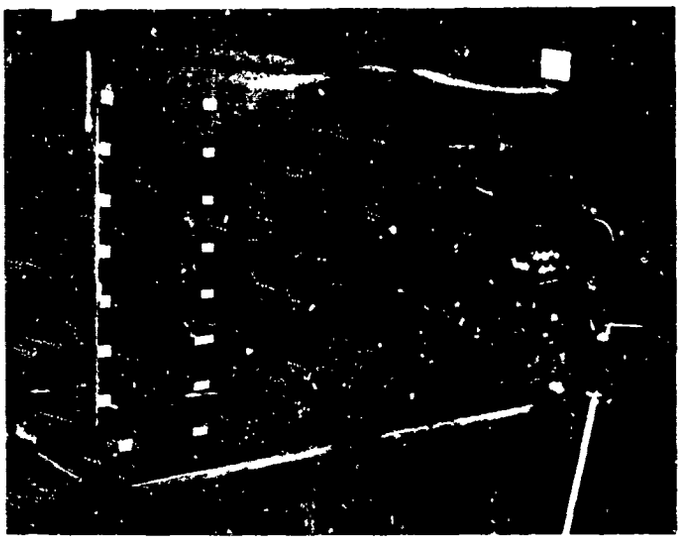

Figure . . . Experimental facility

The operation was then repeated with a succession of fluid strata until the desired overall density deficit from top to bottom was obtained.

After a period of some days ionic diffusion at the interfaces between successive strata smoothed out the density discontinuities and eventually provided a linear density profile in the vertical direction. The density profile was measured by carefully weighing a teflon cylinder (300 cc) submersed at varying depths in the stratified fluid. A density change $\Delta\rho$ in the local average value ρ_o can be determined to an accuracy $\frac{\Delta\rho}{\rho_o} = \frac{\Delta W}{W_o}$ where W is the apparent weight of the teflon cylinder suspended in the fluid. This allowed the density to be determined to better than 1×10^{-4}.

Experiments were conducted in a number of test fluids whose density stratifications $\alpha \left\{ = -\frac{1}{\rho_o}\frac{\partial\rho_o}{\partial z} \right\}$, ranged between $5\times10^{-3}\text{cm}^{-1}$ and $5\times10^{-4}\text{cm}^{-1}$. Thus the Brunt-Väisälä periods, $= 2\pi/(\alpha g)^{\frac{1}{2}}$, for the stratified fluid mixes used in our experiments were in the range between 3 and 10 seconds.

Internal-gravity waves were excited in the stratified test mix by one of two methods. In a series of preliminary experiments a sphere was suspended in the test tank and using a small D.C. motor the sphere was allowed to oscillate vertically at a controlled amplitude and frequency. Measurements were made of the amplitude and frequency of waves as a function of angle from the axis of motion of the oscillating sphere. The results of these experiments are reported in Section 4.4, below.

The main series of experiments in this investigation were conducted by releasing a small volume of buoyant fluid from a control mechanism on the floor of the plexiglas tank. The release mechanism has a facility for refilling with buoyant fluid from beneath the tank; the buoyant fluid is then retained in a hemispherical volume by a sliding lid on top. The lid is opened using a draw cord which is led through guides on the tank floor and up the end walls of the tank to allow manual control from outside the tank. The lid is spring loaded

to allow a controlled opening time. Ethyl or methyl alcohol were generally used as the buoyant fluid due to their low density and good miscibility with water, and in some cases the alcohol was dyed to enhance visualization of the source region.

4.2.2 Internal-Gravity Wave Visualization

The wavefields generated in the test tank were visualized by using neutrally buoyant polystyrene beads dispersed through the stratified fluid mixture. These beads were purchased in the unexpanded state but were then thermally treated to produce varying degrees of expansion in accordance with the requirements for a particular experiment. Samples of beads within quite narrow density ranges are thus obtained and an even distribution of beads can be dispersed throughout the density stratified mixture. Wave propagation in the stratified test fluid may then be observed by examining the motion of individual beads which characterize the motion of the surrounding fluid.

The wavefield created is a three-dimensional one and in order to simplify the interpretation of data, observations were made on a thin two-dimensional characteristic section of the wavefield. This was done by conducting the experiments in a darkened laboratory with a collimated light beam illuminating only a thin vertical section of the test fluid through the axis of symmetry for the experiment. The polystyrene beads act as excellent light scattering centers and their movements were recorded using a 16 mm cine camera.

4.3 THEORY

4.3.1 Fundamental Equations

Internal gravity waves in an incompressible stratified fluid are governed by hydrodynamic equations:

$$\rho \frac{\bar{Du}}{Dt} = - \nabla p - g\rho \bar{e}_z \qquad (1)$$

$$\nabla \cdot \bar{u} = 0 \tag{2}$$

$$\frac{D\rho}{Dt} = 0 \tag{3}$$

Let $p = p_o(z) + p_1$, $\rho = \rho_o(z) + \rho_1$ where p_1, ρ_1 are small. Then for small displacements

$$\bar{u} = \frac{\partial \bar{\xi}}{\partial t}, \quad \frac{D\bar{u}}{Dt} = \frac{\partial^2 \bar{\xi}}{\partial t^2} \tag{4}$$

where $\bar{\xi}$ is the particle displacement from its undisturbed position. From (3) and (4) it follows that to first order,

$$\rho_1 + \bar{\xi} \cdot \nabla \rho_o = 0 \tag{5}$$

From (1) it similarly follows that

$$\rho_o \frac{\partial^2 \bar{\xi}}{\partial t^2} = - \nabla p_1 - g \rho_1 \bar{e}_z \tag{6}$$

ρ_1 may now be eliminated from (5) and (6) so that

$$\rho_o \frac{\partial^2 \bar{\xi}}{\partial t^2} = - \nabla p_1 + g \xi_z \frac{\partial \rho_o}{\partial z} \bar{e}_z \tag{7}$$

From Eqs. (2) and (7) it then follows that

$$\rho_o \frac{\partial^2 \bar{\xi}}{\partial t^2} + \rho_o \omega_o^2 \xi_z \bar{e}_z = - \nabla p_1 \tag{8}$$

$$\nabla \cdot \bar{\xi} = 0 \tag{9}$$

where we have defined the Brunt-Väisälä frequency as $\omega_o^2 = - g\rho_o^{-1} \frac{d\rho_o}{dz}$.

4.3.2 Group Velocity Considerations

We will consider a fluid where ω_o is constant and we let

$$\bar{\xi} = \text{Re} \left\{ \hat{\bar{\xi}} \ \rho_o^{-\frac{1}{2}} \ e^{-i\left[\omega t - \bar{k}\cdot\bar{x}\right]} \right\} \tag{10a}$$

$$p_i = \text{Re} \left\{ \rho_o^{\frac{1}{2}} \hat{P} \ e^{-i\left[\omega t - \bar{k}\cdot\bar{x}\right]} \right\} \tag{10b}$$

where ω, $\bar{k}$, $\hat{\bar{\xi}}$, $\hat{P}$ are constants and Re represents the real part of the term following. Then from Eqs. (8) and (9) it follows that

$$- \omega^2 \hat{\bar{\xi}} + \omega_o^2 \hat{\xi}_z \bar{e}_z = - i\bar{k}\hat{P} + \frac{\omega_o^2}{2g} \hat{P} \bar{e}_z \tag{11a}$$

$$i\bar{k} \cdot \hat{\bar{\xi}} + \frac{\omega_o^2}{2g} \hat{\xi}_z = 0 \tag{11b}$$

From Eqs. (11) it follows that

$$\hat{\xi}_x = -\frac{ik_x}{\omega^2}\hat{P} \tag{12a}$$

$$\hat{\xi}_y = \frac{ik_y}{\omega^2}\hat{P} \tag{12b}$$

$$\hat{\xi}_z = \frac{\left[ik_z - \frac{\omega_o^2}{2g}\right]}{\omega^2 - \omega_o^2}\hat{P} \tag{12c}$$

and that ω and $\bar{k}$ are related by the dispersion relation

$$\left(\omega^2 - \omega_o^2\right)\left(k_x^2 + k_y^2\right) + \left[k_x^2 + \frac{\omega_o^4}{4g^2}\right]\omega^2 = 0 \tag{13}$$

For simplicity we will consider $\hat{\xi}_y$ and k_y to be zero. Then the dispersion relation (13) may be written as

$$\omega^2 = \omega_o^2 k_x^2 \left\{k_x^2 + k_z^2 + \left(\frac{\omega_o^2}{2g}\right)^2\right\}^{-1} \tag{14}$$

If the group velocity C_g is interpreted as $C_{gx} = \frac{\partial\omega}{\partial k_x}$, $C_{gz} = \frac{\partial\omega}{\partial k_z}$ we have

$$C_{gx} = \left(\frac{\omega_o^2 - \omega^2}{\omega_o^2}\right)\frac{\omega}{k_x} \tag{15a}$$

$$C_{gz} = -\frac{\omega^2}{\omega_o^2}\frac{\omega k_z}{k_x^2} \tag{15b}$$

Using Eqs. (14) and (15) to eliminate k_x and k_z we find

$$C_{gx}^4 = \frac{4g^2\left(\omega_o^2 - \omega^2\right)^3}{\omega_o^8}\left[C_{gx}^2 - \left(\frac{\omega_o^2 - \omega^2}{\omega^2}\right)C_{gz}^2\right] \tag{16}$$

We now let θ be the group velocity direction relative to the vertical axis, such that $C_{gx} = C_g \sin\theta$, $C_{gz} = C_g \cos\theta$ and find that

$$C_g^2 = \frac{4g^2\left(\omega_o^2 - \omega^2\right)^3}{\omega_o^8}\left[\frac{\omega^2 - \omega_o^2\cos^2\theta}{\omega^2\sin^4\theta}\right] \tag{17}$$

Thus in order to have propagation, one must have $\omega_o^2\cos^2\theta < \omega^2 < \omega_o^2$.

From Eq. (17) it is seen that for a fixed group velocity direction the group velocity versus frequency curve is of the form sketched in Fig. 2.

4.3 3 Particle Trajectories

From Eqs. (12) we can write

$$\xi_x = -\frac{k_x}{\omega^2} A\cos(\omega t - \phi_o) \tag{18a}$$

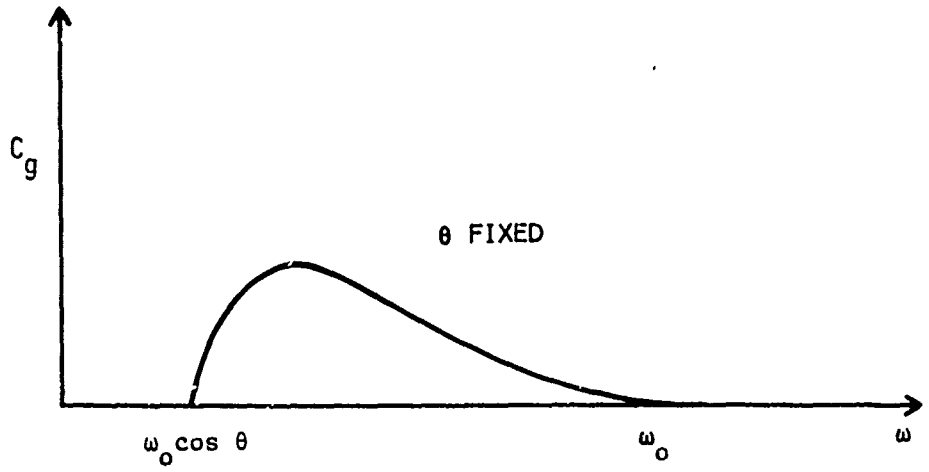

Figure 2. Sketch of group velocity C_g versus frequency ω for a fixed group velocity direction

$$\xi_z = \frac{k_z}{\left(\omega^2 - \omega_o^2\right)} A \cos(\omega t - \phi_o) + \frac{\omega_o^2/2g}{\left(\omega^2 - \omega_o^2\right)} A \sin(\omega t - \phi_o) \qquad (18b)$$

where A and ϕ_o are constant for any given fluid particle.

Writing

$$\alpha = \frac{1}{\omega} \frac{\left(\omega_o^2 - \omega^2\right)}{\omega_o^2 C_{gx}} A \quad , \qquad (19a)$$

$$\gamma = \frac{\left(\omega_o^2 - \omega^2\right)}{\omega\omega_o^2} \frac{C_{gz}}{C_{gx}^2} A \qquad (19b)$$

$$\delta = -\frac{1}{\left(\omega_o^2 - \omega^2\right)} \frac{\omega_o^2}{2g} A \qquad (19c)$$

we derive from Eqs. (14), (15), and (18) that the particle path is given by

$$(\delta^2 + \gamma^2)\ \xi_x^2 + \alpha^2 \xi_z^2 - 2\alpha\gamma\xi_x\xi_z = \alpha^2\delta^2 \qquad (20)$$

which is the equation of an ellipse. As illustrated in Fig. 3a, the direction of the major axis of this ellipse is in general not coincident with the group velocity vector, C_g. The inclination ϕ of the major axis of the ellipse with the vertical may be defined by $(0 < \phi < \pi/2)$

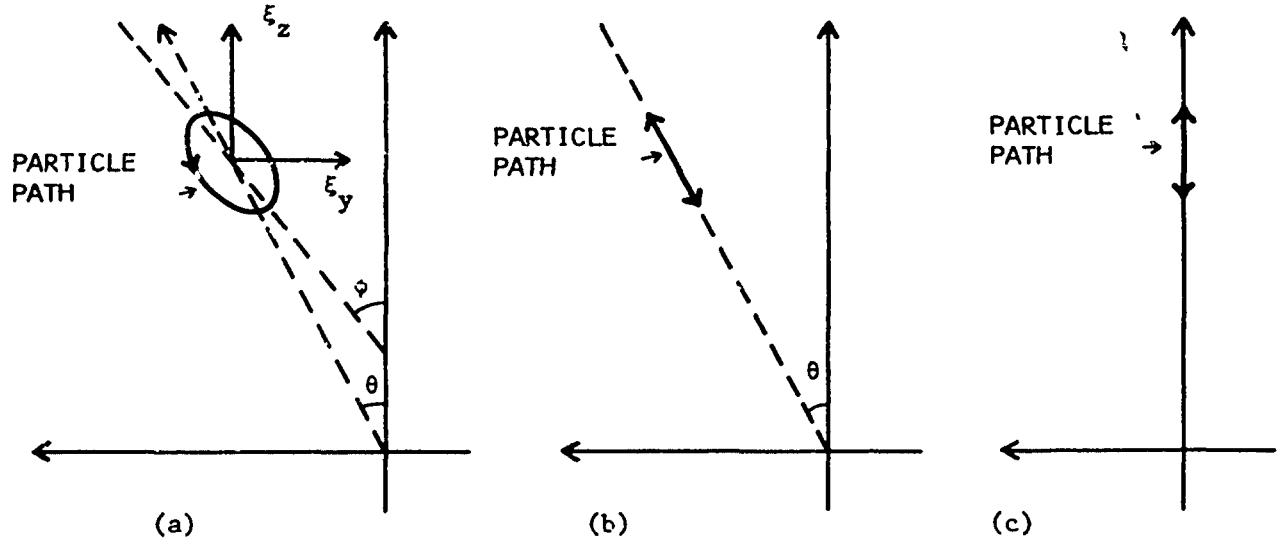

Figure 3. Illustrations of predicted particle trajectories in internal gravity wave. (a) General case; (b) $\omega = \omega_o \cos\theta$; (c) $\omega = \omega_o$.

$$\frac{1}{2} \tan 2\phi = \frac{\gamma\alpha}{\delta^2 + \gamma^2 - \alpha^2} \tag{21}$$

and the ratio L_2/L_1, where L_2, L_1 are the semi-major and semi-minor axes of the ellipse, respectively, may be written as

$$\left(\frac{L_2}{L_1}\right)^2 = \frac{(\alpha^2 + \gamma^2 + \delta^2) \cos 2\phi + (\delta^2 + \gamma^2 - \alpha^2)}{(\alpha^2 + \gamma^2 + \delta^2) \cos 2\phi - (\delta^2 + \gamma^2 - \alpha^2)} \tag{22}$$

Substituting from (19) into (21) we find that

$$\frac{1}{2} \tan 2\phi = \frac{\omega_o^2 - \omega^2}{2\omega^2 - \omega_o^2} \cot \theta \tag{23}$$

Theoretical arguments not presented here indicate that a source of frequency ω radiates most strongly near the angle $\theta = \pm \cos^{-1}(\omega/\omega_o)$ (PIERCE, A. D., 1963). At precisely this angle, Eq. (17) shows the group velocity is zero. However, at angles only slightly different from this value, the group velocity has a finite value and the amplitude is expected to be maximum. For $\omega^2 \approx \omega_o^2 \cos^2\theta$, Eq. (23) reduces to:

$$\tan 2\phi = \tan 2\theta \tag{24}$$

which is satisfied by

$$\phi = \theta \ . \tag{25}$$

Equation (22) may be simplified and in general can be written as

$$\left(\frac{L_1}{L_2}\right)^2 = \frac{\cos 2\phi + \left\{1 - \left(\frac{2\omega^2}{\omega_o^2}\right)\right\}}{\cos 2\phi - \left\{1 - \left(\frac{2\omega^2}{\omega_o^2}\right)\right\}} \tag{26}$$

Thus in the case where $\omega^2 \to \omega_o^2 \cos^2\theta$, then $L_1 \to 0$ and the particle trajectory becomes a straight line whose orientation is in the direction of θ (= ϕ). See Fig. 3b.

In the special case of $\theta \simeq 0$, the only propagating frequency is ω_o, so $L_1 \to 0$, and $\phi = 0^o$. Since the straightline orbits are in the direction of ϕ they will thus be aligned in the vertical direction. See Fig. 3c. At the other extreme case of horizontal propagation, as $\theta \to 90^o$, ϕ may go either 0^o or 90^o depending on whether ω^2 is less than or greater than $\omega_o^2/2$ and elliptical trajectories should in general be observed in the horizontal direction.

Combining Eqs. (23) and (26) we can eliminate ω^2/ω_o^2 to obtain

$$\tan\theta = \frac{1}{\sin 2\phi}\left\{\frac{1 + (L_1/L_2)^2}{1 - (L_1/L_2)^2} - \cos 2\phi\right\} \tag{27}$$

Thus if one measures ϕ and the ratio L_2/L_1 for an observed particle trajectory, it is possible to compute θ without explicitly taking the frequency into account. (This presumes $0 < \theta < 90^o$, $0 < \phi < 90^o$.).

One other result which should be mentioned is the sense in which particles move around elliptical orbits. One may note from Eqs. (18) that, given $\omega^2 < \omega_o^2$, $k_x > 0$, $k_z < 0$ ($C_{gx} > 0$, $C_{gz} > 0$) that $d\xi_z/dt$ is negative when ξ_x has its maximum value. In this case the

orbits would appear clockwise if the source is to the lower left of the observer. In a similar manner, the orbits would be counter clockwise if the source is to the lower right.

4.4 RESULTS

4.4.1 Bobbing Sphere Experiments

A series of preliminary experiments was carried out employing an oscillating sphere as the localized disturbance in a stratified fluid. A schematic illustration is presented in Fig. 4. Sphere sizes from 0.5- to 2.5-inch diameters were used and oscillation frequencies from approximately one-third to one times the Brunt-Väisälä frequency were examined. A 16 mm cine camera recorded the movement of the sphere and the wave patterns indicated by the particle motions, viewing only a vertical two-dimensional plane as described in Section 4.2.

Analysis of the data consisted of plotting the movement of the neutrally buoyant beads at various locations in the wavefield. The wave pattern was clearly observed to take the form of symmetrical "jet" regions on either side of the oscillating source, in the shape of an X as reported by MOWBRAY and RARITY, 1967. The angle of inclination of the gravity wave jet regions was found to vary closely as $\theta = \cos^{-1}(\omega/\omega_o)$ for values of $\omega < \omega_o$ where θ is the jet inclination angle to the vertical. This is consistent with Hurley's results (HURLEY, D. G., 1969) based on the theory of an oscillating cylinder in a stratified fluid. The small change in the Brunt-Väisälä frequency through the density stratified medium is neglected here and a value of ω_o corresponding to its median value is used. Table 1 presents data from some of the measurements showing the correlation between θ and $\cos^{-1}(\omega/\omega_o)$ for a stratified fluid whose Brunt-Väisälä period was 5.75 secs.

A detailed analysis was carried out on the data from one of our oscillating sphere experiments where the actual trajectories of a number of the neutrally buoyant beads were plotted using a stop frame-

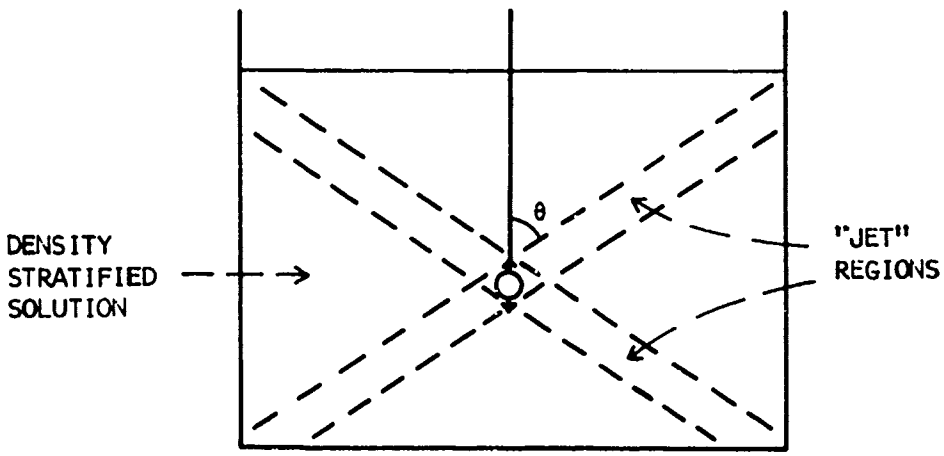

Figure 4. Schematic for Bobbing Sphere Experiment.

TABLE 1

CORRELATION OF MEASURED GRAVITY WAVE JET ANGLE WITH OSCILLATION FREQUENCY OF BOBBING SPHERE. BRUNT-VÄISÄLÄ PERIOD T_o = 5.75 SECS, T = OSCILLATION PERIOD OF SPHERE.

T (secs)	$\cos^{-1} T_o/T = \cos^{-1} \omega/\omega_o$	θ_{meas}
6.5	28^o	29^o
7.0	34^o	32^o
8.0	44^o	40^o
10.4	56^o	56^o
10.9	58^o	58^o
12.8	63^o	61^o
14.2	66^o	66^o

analyst projector. All the particle motions were found to follow straightline paths, and Fig. 5 shows displacement/time plots for two such particles in the gravity wave jet, spaced azimuthally but at equal radial distances from the oscillating source. These clearly indicate the phase change across the jet dimension and the aggregration of such data points across the jet at a fixed radial distance from the source gives a measurement of the wavelength. In our experiments this wavelength was found to agree within 15% with the diameter of the oscillating source region which was defined as the sphere diameter plus the amplitude of the imposed oscillation.

The displacement/time plots for the individual particles give measurements of the wave period and amplitude at all observed parts of the jet region. The wave amplitude tended to be maximum at the center region of the jet, falling off fairly slowly at first away from the jet center line and then quite rapidly at the jet edges. The decay of wave amplitude with increasing range R from the source seems to fall off approximately as $1/\sqrt{R}$ as might be anticipated on the grounds of the following simple consideration: it is observed that the gravity wave jet thickness L and angle of inclination θ to the vertical are constant. Thus from Eq. (17) the group velocity is constant. Energy conservation requires $\hat{E}C_g S$ = const., where $\hat{F}$ the energy density in the jet and S is the area of the jet normal to the group velocity. $S = 2\pi RL \sin\theta$ and the energy density will vary as A^2 where A is the gravity wave amplitude. Thus one would expect A to vary as $1/\sqrt{R}$. Data are presented in Fig. 6 showing measurements of the wave amplitude in the jet at different ranges R from the bobbing sphere. Also shown is the predicted variation as $R^{-\frac{1}{2}}$.

The measured periods for all particles examined fell within the range 11.2 - 12.1 seconds for a mean value of 11.6 seconds. The known source period in this case was 11.5 seconds. The average angle of inclination of the gravity wave jet region, defined by the

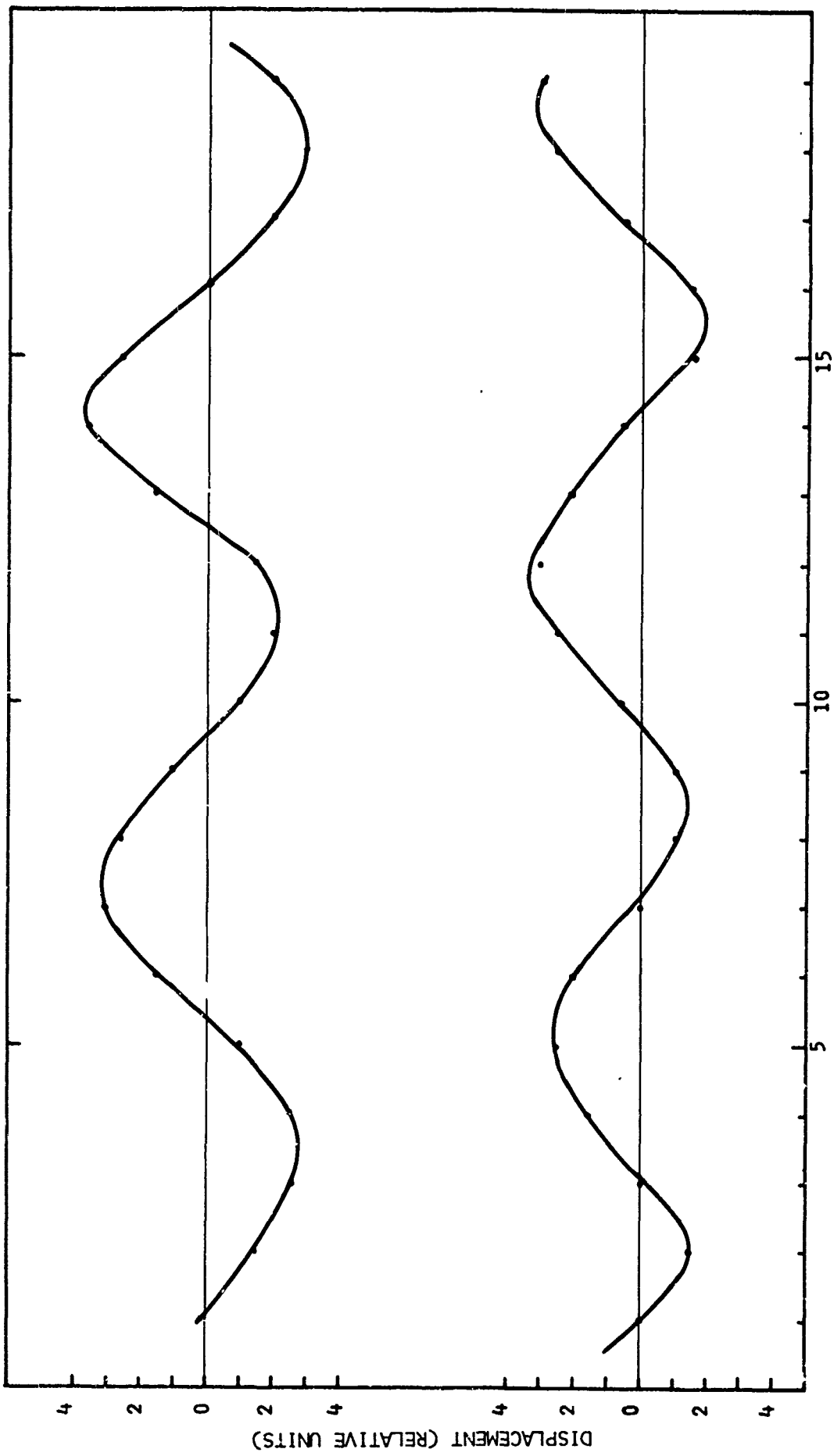

Figure 5. Displacement/time plots for two particles in the gravity wave jet in bobbing sphere experiment. Both particles are at same radial distance from sphere but are separated azimuthally. Note the phase difference.

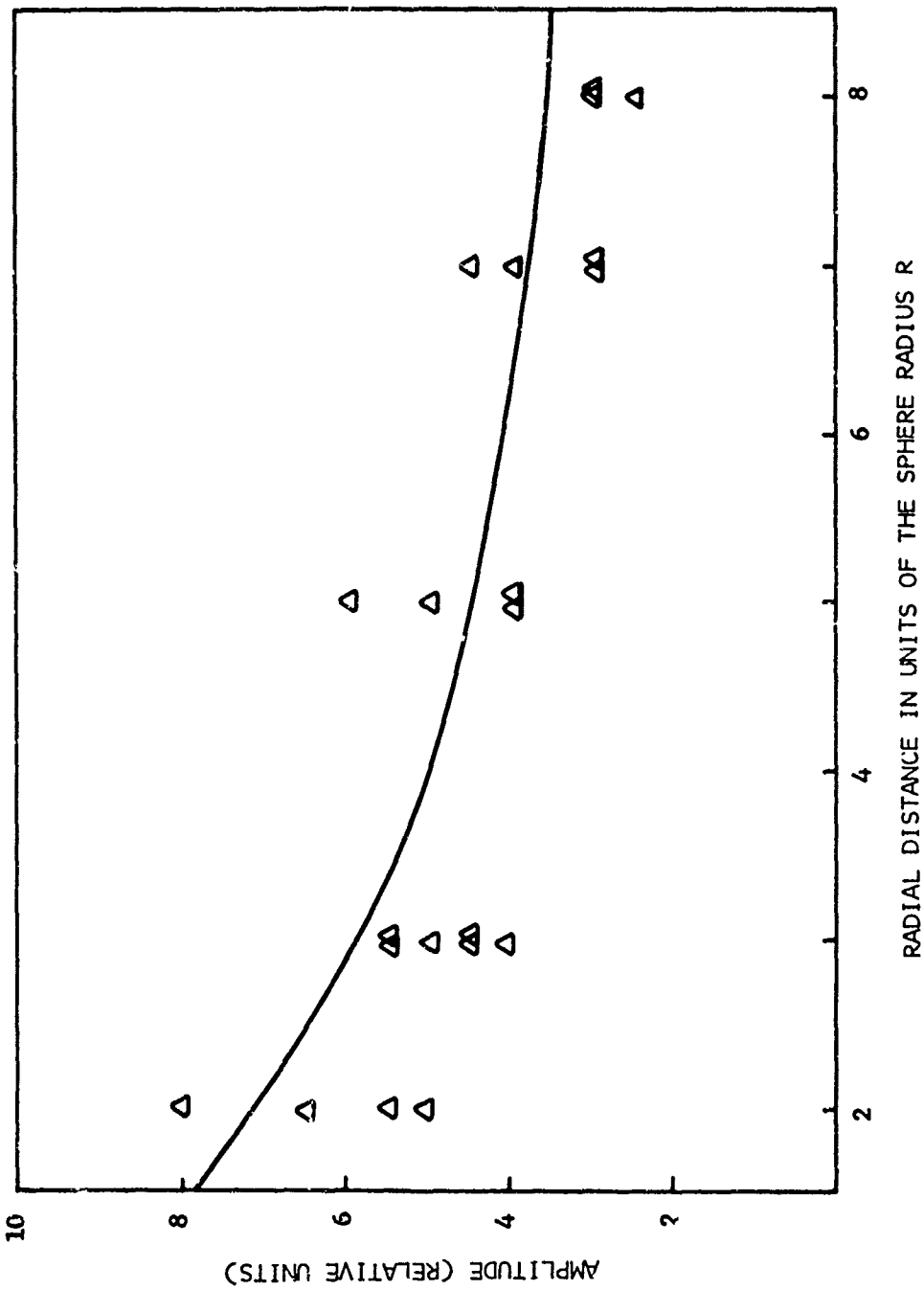

Figure 6. Decay of gravity wave amplitude in the jet with distance from the bobbing sphere. The full line curve shows the decay rate for $A \sim 1/\sqrt{R}$.

bounds within which measurable particle displacements were observed, was 58^{o} from the vertical. This agrees with the value of 58^{o} derived from $\cos^{-1}\omega/\omega_{o}$ for the same experiment.

It was also found that the inclination of the straightline particle paths likewise averaged 58^{o}. This is consistent with the theoretical analysis of Section 4.3 which predicts straightline trajectories aligned in the group velocity direction if $\omega = \omega_{o} \cos \theta$. Illustrative data are presented in Table 2.

4.4.2 Buoyant Release Experiments

A number of experiments were carried out to visualize the wavefield generated by the motion of a buoyantly rising volume of fluid in a stratified environment. Most of the data analyzed was for experiments where a small test volume of alcohol was released at the tank bottom into a stratified salt solution whose stratification, α, was 5×10^{-4} cm^{-1}. The same visualization technique was employed as described above where a cine film was taken of the motion of neutrally buoyant beads in a two-dimensional vertical plane passing through the release point of the buoyant fluid.

Due to the rapid entrainment by the buoyant fluid of the heavier brine solution, stabilization of the rising fluid tended to occur at relatively low levels in the test tank. Thus observations were mainly made on the upward directed waves which provided a longer wave path before reflections at the tank side walls or the top surface of the stratified fluid interfered with the observations.

Whereas in the experiments with the bobbing sphere when an observer could clearly distinguish the wave "jet" regions of the wavefield, in the case of a buoyant fluid release the wave pattern appeared considerably more complex. General observations were made on a number of buoyant releases and some were analyzed in detail; results are presented below.

TABLE 2

MEASURED VALUES OF THE INCLINATION OF PARTICLE STRAIGHTLINE TRAJECTORIES IN A BOBBING SPHERE EXPERIMENT. $\cos^{-1}(\omega/\omega_o) = 58^\circ$

Particle Number	Measured Inclination, θ	Particle Number	Measured Inclination, θ
1	58	9	63
2	56	10	64
3	59	11	57
4	55	12	58
5	54	13	57
6	56	14	59
7	61	15	55
8	64	16	

Distribution of Gravity Wave Frequency

In the case of the bobbing sphere experiments, the period for all particles observed within the wave jet region appeared to be constant and equal to the sphere oscillation frequency, within the scatter of the measurements. With the buoyant fluid release, however, a wide spectrum of wave frequencies was observed. No discernible gravity wave motions were detected during the rise of the buoyant fluid, the waves observed seemed to be generated subsequent to the rise, emanating from the oscillatory motion of the fluid around its stabilization height. Particle trajectories were plotted for various parts of the wavefield and these showed periods varying from the Brunt-Väisälä period to three to four times the Brunt period for waves propagating at angles close to the horizontal. It became difficult to resolve waves with periods longer than this which may propagate at even shallower angles but there was evidence of a non-periodic motion in the horizontal direction, assumed to be associated with the horizontal spread of the buoyant plume at stabilization height.

The main reason for the differences between the wavefields generated by the bobbing sphere and by the buoyant release is that the source region in the latter case represents an inhomogeneous and transient source. As a result, during the oscillatory phase of the stabilizing fluid the trajectory of an individual particle in the wavefield may be observed to vary in time. For example, a particle executing an elliptical orbit may subsequently change to a different elliptical orbit, or may for a time be observed to follow a straightline path. Figure 7 shows sketches of some actual particle trajectories recorded for a buoyant release experiment.

The overall observation time for most of our buoyant release experiments was usually four or five times the Brunt-Väisälä period for the stratified fluid. Since the buoyantly rising test fluid appeared to stabilize after approximately two oscillations at close to Brunt frequency, this meant that our observation time lasted typically

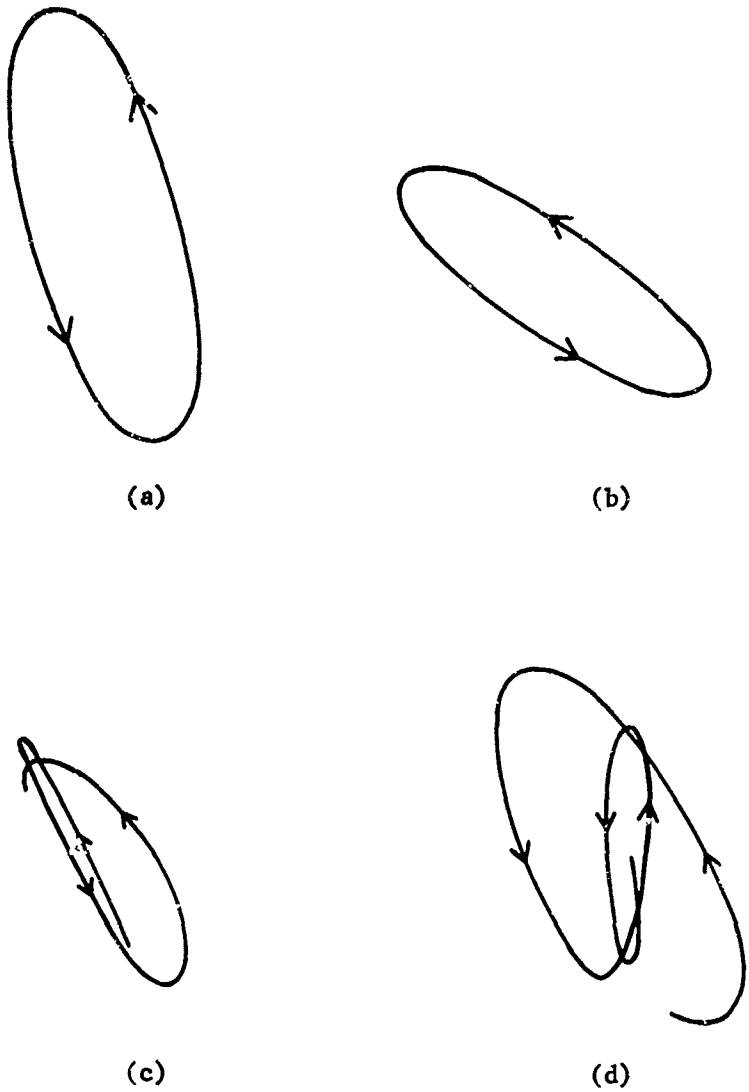

Figure 7. Particle trajectories from analysis of buoyant release experiment. (a) - (c) are from the same experiment; (d) is at late time for another experiment.

two to three periods after the main source motion had ceased. Towards the end of this observation time there were generally indications, and in one experiment very clear evidence, that the particle motions eventually tended to straightline paths in the vertical direction at the Brunt-Väisälä frequency. Such a case is illustrated by the particle trajectory in Fig. 7d. This is in accord with the theoretical argument that the strongest later arrivals from a broadbased transient source should be at Brunt's frequency since the group velocity goes to zero with zero slope at that frequency. Also the vertical trajectories at $\omega = \omega_o$ are consistent with the analysis of Section 4.3.

The direction of the particle motions around their elliptical orbits was observed to be clockwise or counter clockwise in agreement with the predictions of Eqs. (18), as described in Section 4.3.

It follows from Eq. (26) that if a particle trajectory is a straightline path (i.e. $L_1 = 0$), then $\omega^2 = \omega_c^2 \cos \phi$. This is borne out by the data presented in Fig. 8 where the data points relate only to particles observed to be executing straightline paths in the wavefield generated by a buoyant fluid release.

In the more general case of an elliptical particle trajectory, such as shown in Fig. 7a, ϕ and L_1/L_2 may be measured. Then Eq. (27) provides the value of θ which indicates the direction of the source region. From a number of such observations the location of the source may of course be determined by the intersection of the "θ" lines. In our experiments the volume dimensions of the oscillating source region are not specifically defined and it was not possible to critically assess the accuracy of θ values calculated from Eq. (27). However, in general the predicted values were in very good agreement with expectations based on a knowledge of the general location of the source region. Quantitative correlation was difficult because our observation field only extended to about eight or ten times the source region dimensions. Thus a line joining a particle location in the wavefield to the source volume could encompass a fair range of values for θ.

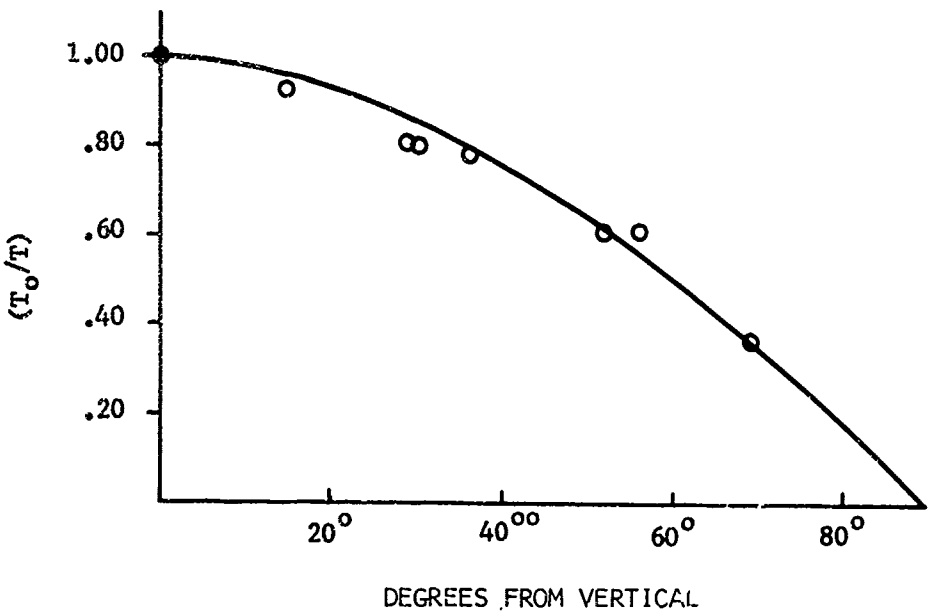

Figure 8. (T_c/T) as a function of particle path inclination to the vertical for straightline trajectories observed in buoyant release experiment. Solid curve is $\cos^{-1}(T_o/T)$.

Description of Gravity Wave Amplitude

Due to the transient nature of the gravity wavefield generated in a buoyant release experiment, it was not feasible to confirm the decay of amplitude with increasing distance from the source region, as was done for the bobbing sphere experiments. However, there is no apparent reason why the decay should differ markedly from the $1/\sqrt{R}$ form observed in the bobbing sphere experiments.

Data was obtained to indicate the variation of gravity wave amplitude with azimuthal angle. Figure 9 presents data showing the variation of the vertical component of gravity wave amplitude with azimuthal angle. This vertical displacement is proportional to the potential energy in the wave. It is seen that the vertical displacement is a maximum directly above the oscillating source region (where, however, the group velocity C_g falls to zero) and falls to a minimum in the horizontal direction.

Rise Time to Stabilization

Table 3 shows the results of measurements made of the rise time for buoyant releases. The rise time is defined as the time interval from release of the buoyant fluid until the top surface of the stabilizing fluid is first observed to fall back in an oscillation about the stabilization height. Typically the stabilizing fluid is observed to undergo about two oscillations before its vertical motion finally comes to rest.

It is seen that the rise time appears to be about 0.85 times the Brunt-Väisälä period for the stratified fluid.

TABLE 3

RISE TIME TO STABILIZATION OF BUOYANT FLUID RELEASES

Release Number	Measured Rise Rise T_R (secs)	T_R/T_o
11-3	8.0	0.82
11-4	8.3	0.85
11-5	8.3	0.85
12-2	8.0	0.82
11-3	8.3	0.85
12-5	8.3	0.85
12-6	8.0	0.82
12-7	9.0	0.92

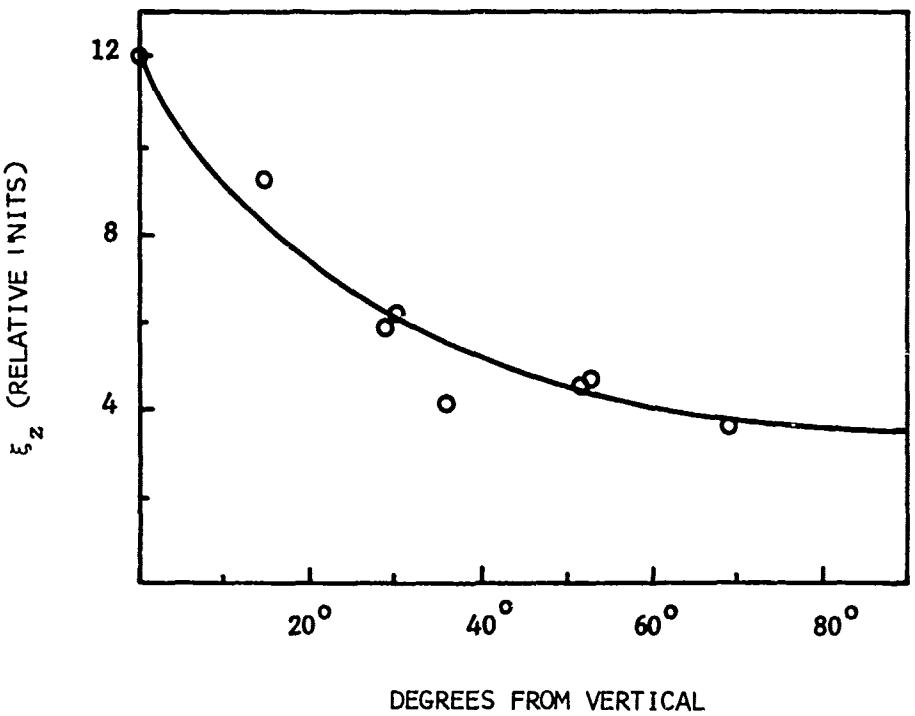

Figure 9. Gravity wave vertical amplitude ξ_z as function of azimuthal angle for fixed radial distnace in buoyant release experiments.

4.5 CONCLUSIONS

Experiments have been carried out to investigate the internal gravity waves generated in an incompressible density stratified medium (a) by the forced oscillation of a spherical body suspended in the stratified medium, and (b) by the motion of a buoyantly rising miscible fluid. The gravity wave motions were analyzed by observing the detailed motion of small neutrally buoyant beads dispersed throughout the stratified medium, and agreement was found between the observations and the theoretical predictions presented in Section 4.3. Observations were also made on the rise to stabilization of the buoyant miscible fluid, and it was found that the rise time to stabilization height was about 0.85 times the Brunt-Väisälä period for the stratified fluid.

The gravity wavefield generated by the motion of a buoyant fluid was observed to be inhomogeneous and transient in nature. However, the theory permits identification of the location of an unseen source of internal gravity waves, if measurements are made of only two characteristics of fluid particles' trajectories, viz: the inclination of the major axis of particle motion, and the ratio of major to minor axis for its (in general) elliptical orbit.

5. REPORT CONCLUSIONS

Conclusions are given below for: (1) Modeling of nuclear sources of acoustic-gravity waves producing ionospheric disturbances. (2) The experimental investigation of internal waves produced by the buoyant rise of a fluid element.

5.1 MODELING OF NUCLEAR SOURCES

(a) Observations of short period ionospheric disturbances following nuclear explosions seem to be caused by the portion of the shock front which is reflected from the 100-120 km altitude level. This identification is made because the periods contained within the shock when it reaches this altitude level are the order of the observed ionospheric periods, that is, about a minute.

(b) Because of the above identification we expect the short periods to scale with explosion parameters in the same way as does the shock positive phase duration at the 100-120 km altitude level. The ionospheric periods should therefore be proportional to the cube root of yield and essentially independent of height of burst.

(c) The origin of ionospheric disturbances with periods exceeding 10 minutes is a complex problem since both the upward going shock and the rising fireball are possible hydrodynamic sources. The mechanism described by GREENE and WHITAKER, 1968, for the generation of long period ionospheric waves involves a refraction of the upward going shock at the 100-120 km altitude level. This results in a transfer of energy from the shock to a horizontally propagating disturbance which is left behind. The Greene-Whitaker mechanism is generally operative since conditions for this shock refraction are a permanent feature of the atmosphere. However, for yields in excess of about a megaton the energy available in fireball rise for the production of long period disturbances exceeds that available in the upward going shock.

(d) The fireball is most efficient in the generation of long period acoustic-gravity waves when it has reached its terminal altitude

and is approaching hydrodynamic equilibrium with the atmosphere. It may then undergo vertical oscillations with a period somewhat larger than the Brunt-Väisälä period. The efficiency of wave generation by this mechanism is very sensitive to ambient conditions at the tropopause as well as to burst parameters. In particular nuclear clouds which undergo rapid spreading upon stabilization appear to be inefficient wave generators. In theory, and this is supported by laboratory experiments, the terminal phases of fireball rise, when the mechanism is efficient, produce a wave spectrum with amplitudes peaked at one to two times the Brunt-Väisälä period. These periods propagate at relatively steep angles to the horizontal and would primarily affect the ionosphere near the burst. burst. Whether significant wave amplitudes could be produced at much longer periods is presently unknown as is the question of whether these long periods, which propagate at shallow angles to the horizontal, would be prevented by atmospheric refraction from reaching ionospheric levels.

5.2 EXPERIMENTAL INVESTIGATION OF INTERNAL WAVES

Experiments were carried out to simulate the gravity wavefield generated by a fireball's rise to stabilization. In essence, the experiment consisted of the release of a small volume of a buoyant fluid at the bottom of a density stratified tank. The fluid was observed to rise to stabilization height where it typically underwent about two oscillations at near the Brunt frequency and gravity waves generated by the motion of the buoyant fluid were observed using neutrally buoyant beads dispersed throughout the density stratified fluid.

The gravity wavefield was found to be generated mainly by the oscillatory motion of the fluid at stabilization height and was observed to be inhomogeneous and transient in nature. The distribution of gravity wave frequency and amplitude with azimuthal angle were identified, and for comparison similar data was discussed for experiments where the source was a set frequency oscillating sphere. The detailed motion of individual fluid elements was observed to agree with theoretical predictions presented in Section 4.3. It was also shown that if measurements are made on only

two characteristics of fluid particle trajectories, viz: the inclination of the major axis of the particle motion, and the ratio of major to minor axis for its (in general) elliptical orbit, then the location of an unseen source of the gravity waves may be identified.

6. REFERENCES

BAKER, D. M., 1968, "Acoustic Waves in the Ionosphere Following Nuclear Explosions" in Acoustic-Gravity Waves in the Atmosphere, T. M. Georges, Ed., U. S. Government Printing Office, pp. 79-86.

BAKER, D. M. and K. DAVIES, 1968, "Waves in the Ionosphere Produced by Nuclear Explosions," J. Geophys. Res. 73, 448.

BARRY, G., 1963, "Ray Tracings of Acoustic Waves in the Upper Atmosphere," J. Atmos. Terrest. Phys. 25, 621.

DARWIN, Sir Charles, 1953, "Note on Hydrodynamics," Proc. Camb. Phil. Soc. 49, 342.

ECKART, C., 1960, Hydrodynamics of Oceans and Atmospheres, Pergamon Press, New York.

GEORGES, T. M., 1968, "Short-Period Ionospheric Oscillations Associated with Severe Weather," in Acoustic-Gravity Waves in the Atmosphere, T. M. Georges, Ed., U. S. Government Printing Office, pp. 171-178.

GLASSTONE, S., 1964, The Effects of Nuclear Weapons, U. S. Government Printing Office.

GREENE, J. S., Jr. and W. A. WHITAKER, 1968, "Theoretical Calculations of Traveling Ionospheric Disturbances Generated by Low Altitude Nuclear Explosions," in Acoustic-Gravity Waves in the Atmosphere, T. M. Georges, Ed., U. S. Government Printing Office, pp. 45-64.

HERRON, T. J., 1971, "Group Velocities of Atmospheric Gravity Waves," J. Atmos. Sci. 28, 598.

HINES, C. O., 1960, "Internal Atmospheric Gravity Waves at Ionospheric Heights," Can. J. Phys. 38, 1441.

HOOKE, W. H., 1968, "Ionospheric Irregularities Produced by Internal Atmospheric Gravity Waves," J. Atmos. Terres. Phys. 30, 795.

HURLEY, D. C., 1969, "The Emission of Internal Waves by Vibrating Cylinders," J. Fl. Mech. 36, 657.

LAMB, Sir Horace, 1945, Hydrodynamics, Dover Publications, New York.

LEHTO, D. L. and R. A. LARSON, 1969, "Long Range Propagation of Spherical Shockwaves from Explosions in Air," Technical Report: NOLTR 69-88, U. S. Naval Ordnance Laboratory, White Oak, Maryland.

LUTZKY, M. and D. L. LEHTO, 1968, "Shock Propagation in Spherically Symmetric Exponential Atmospheres," Phys. of Fluids 11, 1466.

MEECHAM, W. C., 1968, "Effect of Atmospheric Wind Structure on Shorter Period, Nuclear-Generated Infrasound," J. Geophys. Res. 73, 377.

MOWBRAY, D. E. and B. S. H. RARITY, 1967, "A Theoretical and Experimental Investigation of the Phase Configuration of Internal Waves of Small Amplitude in a Density Stratified Liquid," J. Fluid Mech. 28, 1.

MOWBRAY, D. E. and B. S. H. RARITY, 1967, "The Internal Wave Pattern Produced by a Sphere Moving Vertically in a Density Stratified Liquid," J. Fluid Mech. 30, 489.

PIERCE, A. D., 1963, "Propagation of Acoustic-Gravity Waves from a Small Source Above the Ground in an Isothermal Atmosphere," J. Acous. Soc. Am. 35, 1798.

PIERCE, A. D., 1966, "Propagation Modes of Infrasonic Waves in an Isothermal Atmosphere with Constant Winds," J. Acoust. Soc. Am. 39, 832.

REED, S. G., Jr., 1959, "Note on Finite Amplitude Propagation Effects on Shock Wave Travel Times from Explosions at High Altitude," J. Acous. Soc. Am. 31, 1265.

SCHOOLEY, A. H. and B. A. HUGHES, 1972, "An Experimental and Theoretical Study of Internal Waves Generated by the Collapse of a Two Dimensional Mixed Region in a Density Gradient," J. Fluid Mech. 51, 159.

SCORER, R. D., 1950, "Experiments on Convection of Isolated Masses of Buoyant Fluid," J. Fluid Mech. 2, 583.

THOMAS, J. E., A. D. PIERCE, E. A. FLINN and L. B. CRAINE, 1971, "Bibliography on Infrasonic Waves," Geophysical Journal of the Royal Astronomical Society 26, Nos. 1-4.

TOLSTOY, I., 1963, "The Theory of Waves in Stratified Fluids Including the Effects of Gravity and Rotation," Revs. Modern Phys. 35, 207.

TOLSTOY, I. and J. LAU, 1971, "Generation of Long Internal Gravity Waves in Waveguides by Rising Buoyant Air Masses and Other Sources," Geophysical Journal of the Royal Astronomical Society 26, Nos. 1-4.

TURNER, J. S., 1960, "A Comparison Between Buoyant Vortex Rings and Vortex Pairs," J. Fluid Mech. 7, 419.

WARREN, F. W. G., 1960, "Wave Resistance to Vertical Motion in a Stratified Fluid," J. Fluid Mech. 7, 209.

WU, J., 1969, "Mixed Region Collapse with Internal Wave Generation in a Density Stratified Medium," J. Fluid Mech. 35, 531.